Mechanisms of Permeation and Selectivity in Calcium Channels

Ben Corry,*† Toby W. Allen,* Serdar Kuyucak,† and Shin-Ho Chung*
*Protein Dynamics Unit, Department of Chemistry, and †Department of Theoretical Physics, Research School of Physical Sciences, Australian National University, Canberra, Australian Capital Territory 0200, Australia

ABSTRACT The mechanisms underlying ion transport and selectivity in calcium channels are examined using electrostatic calculations and Brownian dynamics simulations. We model the channel as a rigid structure with fixed charges in the walls, representing glutamate residues thought to be responsible for ion selectivity. Potential energy profiles obtained from multi-ion electrostatic calculations provide insights into ion permeation and many other observed features of L-type calcium channels. These qualitative explanations are confirmed by the results of Brownian dynamics simulations, which closely reproduce several experimental observations. These include the current-voltage curves, current-concentration relationship, block of monovalent currents by divalent ions, the anomalous mole fraction effect between sodium and calcium ions, attenuation of calcium current by external sodium ions, and the effects of mutating glutamate residues in the amino acid sequence.

INTRODUCTION

A central problem in studies of ion permeation through biological membrane channels is to understand how channels can be both highly selective and yet still conduct millions of ions per second. Calcium channels exemplify this problem; they are ubiquitous in excitable cells and extremely selective, selecting calcium over sodium at a ratio of 1000:1 (Hess et al., 1986); yet the picoampere currents they support require $>10^6$ calcium ions to pass per second (Tsien et al., 1987). Unlike potassium channels, which have a narrow selectivity filter and only allow ions of a particular size to pass (Doyle et al., 1998; Allen et al., 1999a, 2000a), calcium channels select between ions of almost identical radius, the Pauling radii of sodium and calcium ions being 0.95 and 0.99 Å, respectively. Moreover, calcium channels are known to admit much larger ions, the largest observed is tetramethylammonium, with a radius of ~2.8 Å (McCleskey and Almers, 1985). Thus, a different mechanism of selectivity from that in the potassium channel must be at play, one that relies on the different charges on the ions. Monovalent ions can permeate the channel in the absence of calcium at much higher levels of conductance than can any divalent ions (Kostyuk et al., 1983; Almers and McCleskey, 1984; Hess et al., 1986; Kuo and Hess, 1993a), but are blocked when the calcium concentration reaches only 1 μM (Kostyuk et al., 1983; Almers et al., 1984). That this block is dependent on membrane voltage (Fukushima and Hagiwara, 1985; Lansman et al., 1986; Lux et al., 1990) and the direction of ion movement (Kuo and Hess, 1993a, b) has been taken as evidence for a multi-ion binding (or selectivity and blocking) site residing in the pore. Four glutamate residues in close proximity are believed to line the pore and to be a component of the selectivity filter of the channel, as point mutations of these change the characteristics of selectivity (Yang et al., 1993; Kim et al., 1993; Ellinor et al., 1995; Parent and Gopalakrishnan, 1995; Bahinski et al., 1997). The glutamate residues are expected to be highly charged and to strongly bind the calcium ions in the channel leading them to block the passage of sodium ions.

A number of theoretical models have been developed to explain permeation and selectivity in the calcium channel. Single-file rate theory models in which ions sequentially hop from one site to another have been used most extensively (Tsien et al., 1987). Because of the difficulty in obtaining both high selectivity and throughput with a single binding site (Bezanilla and Armstrong, 1972), these models originally contained two sites in which repulsion between ions in neighboring sites increases transit rates (Hess and Tsien, 1984; Almers and McCleskey, 1984). As the two-site models could not accommodate the mutation data, a new rate model was recently proposed where a single-site is flanked by lower affinity sites to aid the exit of ions from the central site (Dang and McCleskey, 1998). Other mechanisms involving single sites have also been developed, such as competition between calcium ions for the binding charges (Armstrong and Neyton, 1991; Yang et al., 1993). These rate theory models have provided many useful insights as to how calcium channels may achieve their selectivity with a high throughput. However, they cannot be used to relate the structural parameters of the channel to functional elements (McCleskey, 1999). For example, in these theories no physical distances or shapes are used and there is no direct connection between energy minima used in the theory and physical sites in the pore.

A first attempt to relate the observed properties of the calcium channel to its structure was made with the Poisson-Nernst-Planck (PNP) theory, which uses continuum electrostatics and electrodiffusion equations to calculate channel conductance (Nonner and Eisenberg, 1998). The shortcom-

Received for publication 1 May 2000 and in final form 17 October 2000.
Address reprint requests to Dr. S. H. Chung, Protein Dynamics Unit, Department of Chemistry, Australian National University, Canberra, A.C.T. 0200, Australia. Tel.: 61-2-6249-2024; Fax: 61-2-6247-2792; E-mail: shin-ho.chung@anu.edu.au.
A video segment of animations showing the flow of ions across the calcium channel will be made available upon request.

0006-3495/01/01/195/20 $2.00

ings of the PNP theory as applied to a model calcium channel were pointed out by McCleskey (1999) and Miller (1999). These criticisms have been given a solid foundation in recent comparisons of PNP theory with Brownian dynamics (BD) simulations (Corry et al., 1999, 2000a, b), which show that the mean field approximation used in the PNP theory completely breaks down in narrow channels, such as the calcium channel. The good agreement between the PNP results and the channel data, often put forward as a proof of its validity, is seen in hindsight as a fortuitous outcome of mixing incorrect physics with unrealistic parameter values. For example, the calcium diffusion coefficient used in the PNP fits (10^{-5} times the bulk value) is 10,000 times smaller than the microscopic estimates obtained from molecular dynamics simulations, which suggest at most a 10-fold reduction in calcium diffusion compared to the bulk value (Allen et al., 2000b). Agreement with experiment also relies on the inclusion of ad hoc chemical potentials whose electrostatic origin is not clear.

Failure of the mean field approximation in narrow channels indicates that any theory that aspires to relate channel structure to its function must treat ions explicitly. Because all the atoms in the system are treated explicitly in molecular dynamics, it would provide the ultimate approach to the structure-function problem. Unfortunately, computation of most channel properties (e.g., conductance) using molecular dynamics is still beyond the capabilities of current computers. The only remaining alternative is BD simulations, where water is treated as continuum and only the motion of individual ions is followed via the Langevin equation. The early BD simulations of ion permeation were carried out in one dimension with assumed electric potentials (Cooper et al., 1985; Bek and Jakobsson, 1994), which were not very useful as realistic models of channels. In the past few years we have extended BD simulations to three dimensions, with the electric fields properly calculated from the solution of Poisson's equation (Li et al., 1998; Hoyles et al., 1998a). These realistic BD simulations have been used to describe ion permeation in the acetylcholine receptor (Chung et al., 1998) and KcsA potassium channel (Chung et al., 1999). Multi-ion interactions were found to be instrumental in explaining the high throughput of potassium channels, and are expected to play a similarly significant role in understanding the high conductance of calcium channels.

The aim of this paper is to construct a simple model of the structure of calcium channels and examine its various properties using electrostatic calculations and BD simulations. The parameters in the model are determined from either molecular dynamics or a variational principle that optimizes the quantity in question. Thus there are no free parameters that are fitted to data, nor ad hoc chemical potentials that are arbitrarily chosen. The model relates structural features to functional roles and, as will be seen, successfully predicts many of the observed properties of the calcium channel using only the principles of electrodynamics.

METHODS

Channel model

The crystal structure of calcium channels is not known at present. Nevertheless, through a judicious use of important clues from various experiments one can develop a simplified model of the calcium channel that should be sufficiently accurate for the purposes of electrostatic calculations and BD simulations. The cross-section of the channel model used in this work is shown in Fig. 1 *A*. A three-dimensional shape of the channel is generated by rotating the curves in Fig. 1 *A* about the axis of symmetry (z axis) by 180°. The channel extends from $z = -25$ Å to 25 Å, long enough to span a typical membrane. In constructing this model, we have followed the basic topology of the potassium channel (Doyle et al., 1998); that is, a narrow selectivity filter, connected to a wide chamber that tapers off as it approaches to the intracellular side. One significant difference from the potassium channel is the existence of a relatively short vestibule on the extracellular side with a fairly wide opening. This is suggested by molecular modeling studies (Schetz and Anderson, 1993; Guy and Durell, 1995; Doughty et al., 1995, 1998) of the known amino acid sequences of the calcium channel (Tanabe et al., 1987; Mikami et al., 1989; Williams et al.,

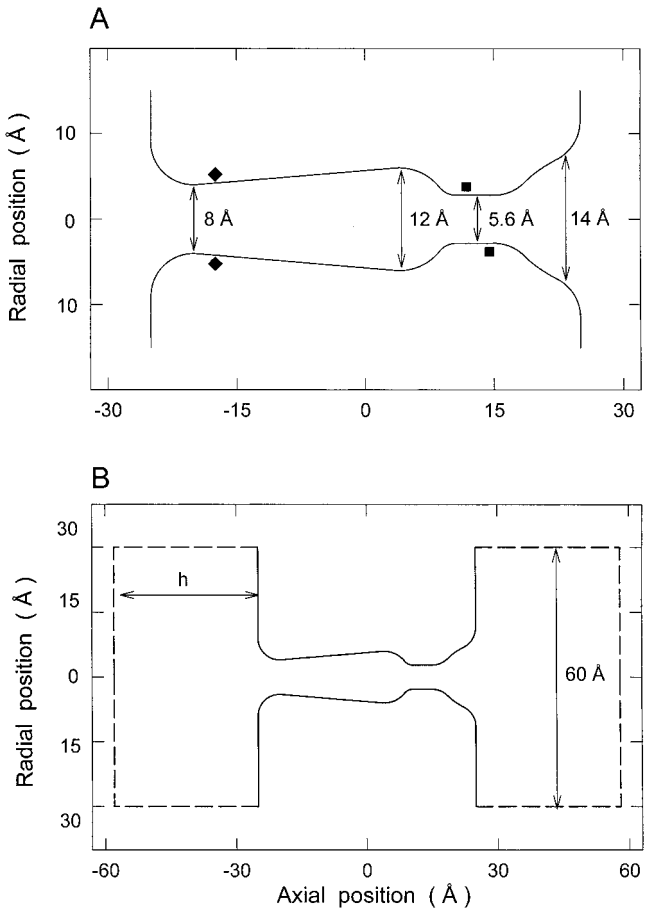

FIGURE 1 Model calcium channel and reservoirs. (*A*) The three-dimensional channel model is generated by rotating the curves about the central axis by 180°. The positions of two of the four glutamate groups are shown by the squares, and the inner end of two of the four mouth dipoles by the diamonds. The other two groups lie into and out of the page. The intracellular end of the channel is on the left and the extracellular side on the right. (*B*) The channel is enclosed with cylindrical reservoirs on either side representing the intracellular and extracellular baths.

1992). A larger external mouth compared to the internal one is required to explain the asymmetry between the inner and outer saturation currents (Kuo and Hess, 1992).

The radius of the selectivity filter is determined from the size of the largest permeable ion (tetramethylammonium) as 2.8 Å (McCleskey and Almers, 1985). Interpretation of the mutation data in reaction rate theories suggests that the four glutamate residues (EEEE locus) in the selectivity filter must be in close proximity in order to form a single binding site (Yang et al., 1993; Ellinor et al., 1995; Bahinski et al., 1997). This is further supported by the voltage dependence of calcium block, which suggests that calcium binds at the same location whether entering the channel from the inside or outside (Kuo and Hess, 1993a). Therefore, we have chosen the length of the selectivity filter to be 5 Å, which is much shorter compared to that in a potassium channel (12 Å). The position of the selectivity filter in the channel is not known, though it is suspected to be toward the external side of the channel, as it is more accessible to ions from the outside of the channel than from the inside (Kuo and Hess, 1993a). Our trials with various positions of the selectivity filter in the channel also confirm this conjecture: when the filter position is further removed from the external mouth, it is not possible to reproduce most of the known properties of calcium channels. The wide chamber near the middle plays a similar stabilizing role to that in potassium channels, providing a water-filled cavity for ions exiting from the selectivity filter (Roux and MacKinnon, 1999).

The highly charged glutamate residues forming the selectivity filter play an essential role in determining the channel conductivity and selectivity, and therefore, choosing their positions and charges correctly is of critical importance. The four glutamate residues are modeled by four fixed charges located in close proximity, but spread asymmetrically in a spiral pattern 1 Å behind the channel wall. The placement of charges in an asymmetric pattern rather than in a ring helps to account for the mutagenesis studies that show the removal of each charge has a different effect on channel conductance. The four charges are located at $z = 10.50$, 11.83, 13.17, and 14.5 Å, and each rotated by 90° from the last (only two are shown in Fig. 1 *A*). Finally, to overcome the large image forces at the intracellular end of the channel we have placed four mouth dipoles, 5 Å in length, with their inner ends 1 Å inside the pore wall at $z = -17.5$ Å. The charges on glutamates and mouth dipoles are optimized to obtain the maximum ionic currents as discussed below. Because we use a rigid protein structure, we do not consider here the possibility of negative charges protruding into the channel and swinging out of the way as ions pass through. We find that such a flexibility of glutamate residues is not required to reproduce experimental data.

The dielectric constant of the channel protein is taken uniformly as $\epsilon = 2$. The dielectric constant of water inside the channel environment is not well known, as it is difficult to determine its value directly from experiments. Recent molecular dynamics simulations of water inside narrow channels have suggested that it may be considerably lower than its bulk value (Sansom et al., 1997). However, BD simulations of ion permeation in potassium channels indicate that current ceases to flow if ϵ in the channel is lower than 40 (Chung et al., 1999). In view of these uncertainties, we have adopted the value of $\epsilon = 60$ that allows large conductance through the model channel. Further justification for this choice will be given later.

Reservoirs

The channel in Fig. 1 *A* is enclosed by cylindrical reservoirs on either side of the membrane that represent the intracellular and extracellular baths (Fig. 1 *B*). The reservoirs have a fixed radius of 30 Å and their height is adjusted to obtain the desired concentration (typically ~33 Å). This length scale (≈4 Debye lengths for 150 mM) is optimal in the sense that the fields of ions outside a 30 Å sphere are totally screened out, and therefore they would have no effect on the dynamics of ions inside the channel. The reservoir boundaries simply serve to confine the ions within the simulation system, which is the easiest way to maintain the average concentrations in the baths at the desired values. Implicit in the use of reservoirs is the assumption that electrolyte solution continues beyond its boundaries. It is worthwhile to emphasize that the reservoir boundaries are not used in the solution of Poisson's equation. That is, we do not fix the potentials at the top and bottom reservoir surfaces, rather they follow from the solution of Poisson's equation as described below.

Scattering of an ion from the boundary wall can be viewed as an ion moving out of the reservoir and another one entering at the same time. In reality, the number of ions in the reservoir will not be constant, but fluctuate around an average value. Such fluctuations have recently been taken into account using a grand canonical Monte Carlo method (Im et al., 2000). Here we use the simpler method because fluctuations in concentration are expected to increase the noise in the current measured from BD simulations but not to affect its average value, which is the observed quantity.

Solution of Poisson's equation

The electric potential ϕ of a configuration of ions and fixed charges in the channel system, represented by the charge density ρ, is found from the solution of Poisson's equation:

$$\epsilon_0 \nabla[\epsilon(\mathbf{r})\nabla\phi(\mathbf{r})] = -\rho(\mathbf{r}), \tag{1}$$

where the dielectric constant $\epsilon(\mathbf{r})$ has different values on either side of the channel boundary. For the proposed boundary in Fig. 1 *A*, Poisson's equation can only be solved numerically. This is achieved using the boundary charge method (Levitt, 1978), where the boundary is divided into small sectors, and each sector is represented by a point charge at its center. For faster convergence and more accurate solutions, we have included the effect of curvature of sectors in the solutions following Hoyles et al. (1996, 1998b). We refer to these references for details of this method.

Implementing different values of ϵ for water in the channel and reservoirs leads to problems in the boundary charge method (Chung et al., 1999). We use instead the same value of $\epsilon = 60$ for water everywhere and incorporate the neglected Born energy difference between the reservoirs and the channel interior as a potential barrier at either channel entrance. The barrier height is estimated from the solution of Poisson's equation using a three-dimensional grid as described elsewhere (Moy et al., 2000). Further description and justification of this approximate way of handling the dielectric constant in BD simulations is given in Chung et al. (1999). We note that while solution of Poisson's equation using a three-dimensional grid avoids the above problem, it is far too slow to be of practical use in BD simulations.

Brownian dynamics

An introduction to BD simulations in one-dimensional channels is given by Cooper et al. (1985). BD simulations have recently been extended to realistic three-dimensional channel geometries (Li et al., 1998; Chung et al., 1998, 1999; Hoyles et al., 1998a). We give a brief description of the method here and focus on new features that have not been discussed before.

In BD, the motion of individual ions is simulated using the Langevin equation

$$m_i \frac{d\mathbf{v}_i}{dt} = -m_i\gamma_i\mathbf{v}_i + \mathbf{F}_R(t) + q_i\mathbf{E}_i + \mathbf{F}_S, \tag{2}$$

where m_i, q_i, and $\mathbf{v}_i$ are the mass, charge, and velocity of the ith ion. In Eq. 1, the effect of the surrounding water molecules is represented by an average frictional force with a friction coefficient $m_i\gamma_i$, and a stochastic force $\mathbf{F}_R$ arising from random collisions. The last two terms in Eq. 2 are, respectively, the electric and short-range forces acting on the ion. The total

electric field at the position of the ion is determined from solution of Poisson's equation, and includes all possible sources due to other ions, fixed and induced surface charges at the channel boundary, and the applied membrane potential. Because solving Poisson's equation at each time step is computationally prohibitive, we store precalculated values of the electric field and potential due to one- and two-ion configurations in a system of lookup tables, and interpolate values from these during simulations (Hoyles et al., 1998a). For this purpose, the total electric potential ϕ_i experienced by an ion i is broken into four pieces

$$\phi_i = \phi_{X,i} + \phi_{S,i} + \sum_{j \neq i}(\phi_{I,ij} + \phi_{C,ij}), \quad (3)$$

where the sum over j runs over all the other ions in the system; $\phi_{X,i}$ is the external potential due to the applied field, fixed charges in the protein wall, and charges induced by these; $\phi_{S,i}$ is the self-potential due to the surface charges induced by the ion i on the channel boundary; $\phi_{I,ij}$ is the image potential due to the charges induced by the ion j; and $\phi_{C,ij}$ is the Coulomb potential due to the ion j. The first three potential terms in Eq. 3 are stored in, respectively, 3-, 2-, and 5-dimensional tables (dimension is reduced by one in the latter two cases by exploiting the azimuthal symmetry of the dielectric boundary).

The short-range forces are used to keep the ions in the system and also to mimic other interactions between two ions that are not included in the simple Coulomb interaction. In order to prevent ions from leaving the system, a hard-wall potential is activated when the ions are within one ionic radius of the reservoir boundaries, which elastically scatters them. For the ion-wall interaction U_{IW}, we use the usual $1/r^9$ repulsive potential

$$U_{IW}(r) = \frac{F_0}{9}\frac{(R_i + R_w)^{10}}{(R_c(z) + R_w - a)^9}, \quad (4)$$

where R_i is the ion's radius, R_w is the radius of the atoms making up the wall, $R_c(z)$ is the channel's radius as a function of the z coordinate, and a is the ion's distance from the z axis. We use $R_w = 1.4$ Å and $F_0 = 2 \times 10^{-10}$ N in Eq. 4, which is estimated from the ST2 water model used in molecular dynamics (Stillinger and Rahman, 1974).

At short ranges, the Coulomb interaction between two ions is modified by adding a potential $U_{SR}(r)$, which replicates effects of the overlap of electron clouds and hydration. Molecular dynamics simulations show that the hydration forces between two ions add further structure to the $1/r^9$ repulsive potential due to the overlap of electron clouds in the form of damped oscillations (Guàrdia et al., 1991a, b). These two effects can be approximately represented by

$$U_{SR}(r) = U_0\{(R_c/r)^9 - \exp[(R - r)/c_e]\cos[2\pi(R - r)/c_w]\}. \quad (5)$$

Here the oscillation length $c_w = 2.76$ Å is given by the water diameter and the other parameters are determined by fitting Eq. 5 to the potentials of mean force given by Guàrdia et al. (1991a, b, 1993, 1996). Fig. 2 *A* shows a plot of the short-range potential for NaCl solution used in our Brownian dynamics simulations. For anion-cation pairs $R_c = r_1 + r_2$, but for like ions the contact distance is pushed further to $R_c = r_1 + r_2 + 1.6$ Å. The origin of the hydration force R is slightly shifted from R_c; by $+0.2$ Å for like ions and by -0.2 Å otherwise. The exponential drop parameter is determined as $c_e = 1$ Å for all ion pairs. Finally, the overall strength of the potential is $U_0 = 16.8$, 8.5, 1.7, 2.5, 0.8, and 1.4 kT for Ca-Cl, Na-Cl, Ca-Na, Na-Na, Ca-Ca, and Cl-Cl pairs, respectively. This potential agrees well with the potential of mean force derived by Guàrdia et al. (1991a, b). The short-range force in Eq. 2 is determined from the derivatives of the potentials in Eqs. 4 and 5.

The BD simulations using this combination of Coulomb and short-range forces accurately mimic the results of molecular dynamics simulations. In Fig. 2 *B* we show the radial distribution functions for Na-Na, Na-Cl, and Cl-Cl pairs obtained from a 2.5 ns BD simulation of a 1.79 M NaCl solution (22 Na^+ and 22 Cl^- ions) confined in a large cylinder with a diameter and height of 30 Å. To avoid the edge effects, ions within 8 Å of the boundary at any time step are excluded from the sampling. As expected, the resulting peaks in the distribution function are located at the minima of the potential of mean force, and also closely match those locations found in the radial distribution functions from molecular dynamics simulations of Lyubartsev and Laaksonen (1995) (indicated by the arrows in Fig. 2 *B*). Similar results are obtained for $CaCl_2$ solutions, but because the molecular dynamics simulation results obtained by different groups vary, a comparison similar to Fig. 2 *B* is not presented for $CaCl_2$.

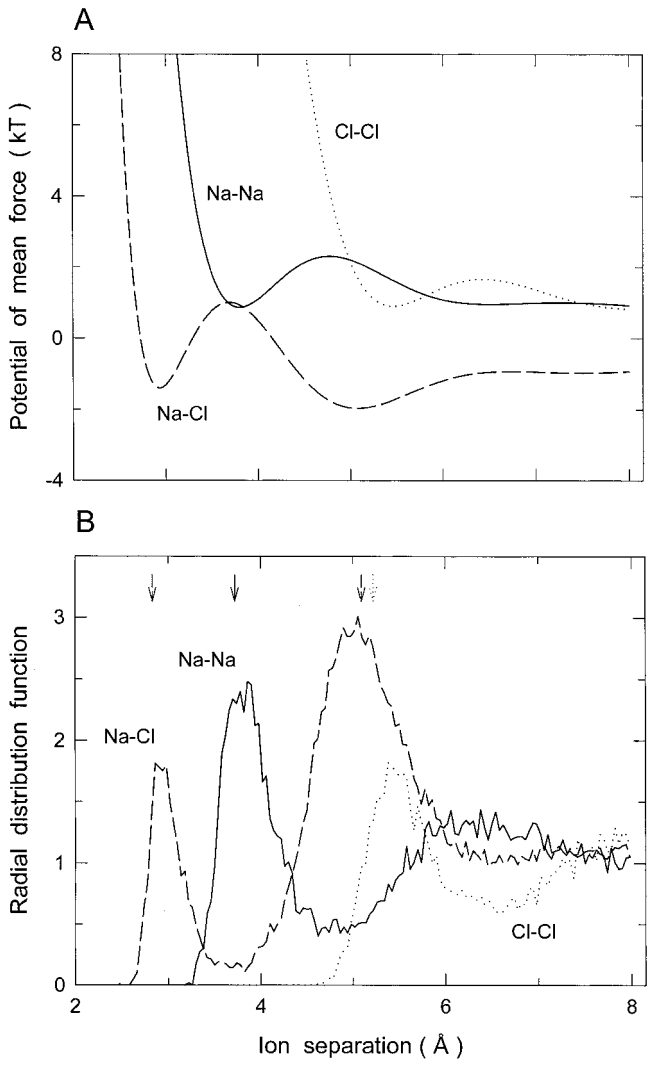

FIGURE 2 Ion-ion forces used in BD simulations. (*A*) The inter-ion potentials for Na^+-Na^+ (*solid line*), Na^+-Cl^- (*dashed line*), and Cl^--Cl^- (*dotted line*) ion pairs are plotted against the ion separation as given by Eq. 5. (*B*) The radial distribution functions for 1.79 M NaCl solution derived from BD simulations (the same line styles as in *A* are used). The locations of the maxima found in the molecular dynamics simulations of Lyubartsev and Laaksonen (1995) are indicated by the arrows at the top of the graph.

We have found that simpler ion-ion interactions used in BD studies of other channels (e.g., Chung et al., 1998, 1999) are not suitable for use in calcium channels. Contrary to the realistic interaction described above, they allow cations to pass each other in the selectivity filter, thus making it impossible to explain the observed blocking of sodium ions by calcium, and vice versa.

The Langevin equation (Eq. 2) is solved at discrete time steps following the algorithm devised by van Gunsteren and Berendsen (1982). To simulate the short-range forces more accurately we use a multiple time step algorithm in our BD code. A shorter time step of 2 fs is used across the channel (between $z = -25$ to 20 Å) where short-range ion-ion and ion-protein forces have the most impact on ion trajectories. Elsewhere, a longer time step of 100 fs is used. If an ion is inside the short time step region at the beginning of a 100-fs period, then that ion is simulated by 50 short steps while the other ions in the long-time regions are frozen to maintain the synchronicity. Simulations under various conditions, each lasting for one million time steps (0.1 μs), are repeated numerous times. Initially, a fixed number of ions are assigned random positions in the reservoirs, with velocities also assigned randomly according to the Maxwellian distribution. The current is determined from the number of ions traversing the channel during the simulation period. To maintain the specified concentrations in the reservoirs, a stochastic boundary is applied: when an ion crosses the channel, say from left to right, an ion of the same species is transplanted from the right reservoir to the left. For this purpose, the ion on the furthermost right-hand side is chosen, and it is placed on the far left-hand side of the left reservoir, making sure that it does not overlap with another ion. The stochastic boundary trigger points, located at either pore entrance, are checked at each time step of the simulation. The sudden disappearance of an ion from the reservoir boundary has a negligible effect on ions in the channel. To give an example, the force between two monovalent ions at 30 Å is 3×10^{-13} N, which is 1000 times smaller than the average random force. The potential change experienced by an ion near the trigger point in the channel is about 3 mV when an ion is removed from one reservoir and placed in the other.

The BD program is written in FORTRAN, vectorized and executed on a supercomputer (Fujitsu VPP-300). The time to complete the simulations depends on how often ions enter the short time step regions. With 48 ions in the system, the CPU time needed to complete a simulation period of 1.0 μs (10 million time steps) is roughly 30 h.

A temperature of 298 K is assumed throughout and a list of the other parameters used in the BD simulations is given in Table 1. (Note that the diffusion coefficient is related to the friction coefficient, γ, in Eq. 2 by the Einstein relation.)

RESULTS AND DISCUSSION

Channel parameters

The three channel parameters that are not known experimentally and need to be determined by other methods are the magnitude of the charges on glutamate residues and mouth dipoles, the dielectric constant of water, and the diffusion coefficient of ions in the channel. A straightforward fit of these parameters to the available data is not very satisfactory, since one is likely to find many possible sets that eventually have to be distinguished on their physical merits. Therefore, we prefer using guiding principles such as optimization or a more explicit theory (e.g., molecular dynamics) in estimating these quantities.

TABLE 1 Parameters used for BD simulations

	Ca^{2+}	Na^{+}	Cl^{-}
Mass (kg)	6.6×10^{-26}	3.8×10^{-26}	5.9×10^{-26}
Bulk diffusion coefficient (m^2s^{-1})	0.79×10^{-9}	1.33×10^{-9}	2.03×10^{-9}
Ionic radii (Å)	0.99	0.95	1.81

The determination of the molecular structure of the proteins may help to find the magnitude of the charge of residues in the channel. In the meantime, we expect that the charges in the channel would have evolved to maximize the transit rate of calcium ions. In Fig. 3 *A* we show the dependence of the calcium current on glutamate charges. The BD simulation results in this figure are obtained using symmetric 150 mM $CaCl_2$ or NaCl solutions with an applied field of -2×10^7 V/m (corresponding to a potential

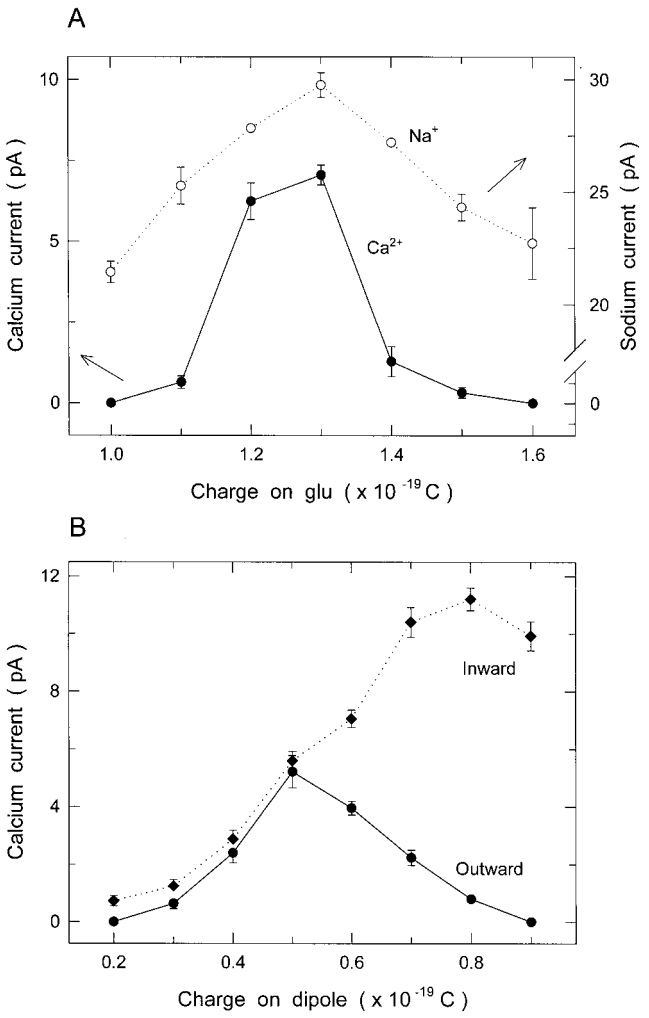

FIGURE 3 Dependence of channel current on fixed charge strengths. (*A*) The current passing through the channel with 150 mM $CaCl_2$ (*filled circles*, *left side scale*) and 150 mM NaCl (*open circles*, *right side scale*) under a -200 mV driving potential is plotted against the charge on each of the glutamate groups. The magnitude of the charge on the mouth dipoles is fixed at 0.6×10^{-19} C. Filled circles are obtained from a 1.0 μs and open circles from a 0.5 μs simulation period. (*B*) The outward (*filled circles*) and inward (*open circles*) current passing through the channel with 150 mM $CaCl_2$ in the reservoirs and a -200 mV driving force is plotted against the magnitude of the charge on each end of the mouth dipoles. The charge on the glutamates is held at 1.3×10^{-19} C. Results are obtained from a 2 μs simulation period. Error bars in this and following figures have a length of one standard error of the mean and are not shown when smaller than the data points.

of ~ -200 mV producing an inward current). As the charge on the glutamate groups is systematically increased (while the charge on the mouth dipoles is held fixed), the calcium current found from BD simulations sharply increases from zero to a narrow peak at a charge of 1.3×10^{-19} C before dropping steeply again at greater charge strengths. In fact, no calcium current is measured during our simulations if the charges are $<1.0 \times 10^{-19}$ C or $>1.6 \times 10^{-19}$ C. The sodium current also peaks at the same value but conducts over a greater range of glutamate charges, as is shown by the open circles. It is noteworthy that the peak calcium current occurs for such a narrow range of glutamate charges. A fully charged glutamate group has a charge of e (1.6×10^{-19} C). However, in an electrolyte solution the charges are likely to become protonated, leading to a lower effective charge on the residues. (Chen et al., 1996; Morrill and MacKinnon, 1999; Root and MacKinnon, 1994, Chen and Tsien, 1997). As the amount of protonation is not known, we use the optimum value of the glutamate strengths, 1.3×10^{-19} C, for the remainder of this study.

In a similar investigation, the strength of the mouth dipoles is varied while the glutamate charges are held fixed at their optimal value. As shown in Fig. 3 *B*, the outward calcium current is critically dependent on the charge strengths, as in the case of the glutamate residues. The current is maximum when a charge of 0.5×10^{-19} C is placed on each of the four dipoles. A further increase in the dipole strength reduces the current rapidly (*filled circle*, Fig. 3 *B*). In contrast, the inward current exhibits a different dependence on the mouth dipole strength (*open circles*, Fig. 3 *B*). The current increases steeply with the dipole strength and then remains constant with a further increase. In all subsequent simulations, we use a charge of 0.6×10^{-19} C, which falls between the optimum values of inward and outward currents and gives close to the maximum value for each.

Molecular dynamics studies of water in spherical cavities (Zhang et al., 1995) and narrow pores (Sansom et al., 1997) suggest that the dielectric constant ϵ is substantially reduced from the bulk value. The effect of changing the dielectric constant on the results of BD simulations in narrow pores (the potassium channel) has been examined elsewhere (Chung et al., 1999). This study also found that the optimum charge strengths are insensitive to the value of the dielectric constant. The dielectric constant of water in the channel is chosen as $\epsilon = 60$. While this value is rather close to the bulk value, the channel ceases to conduct calcium ions if lower values of ϵ are used. For example, when the dielectric constant ϵ inside the channel is assumed to be 50 and a potential difference of -200 mV is applied, the current across the channel is only 2.4 ± 0.6 pA, compared to 7.1 ± 0.6 pA with $\epsilon = 60$. With a further reduction of ϵ to 40, the current is reduced to 0.4 ± 0.2 pA (during a simulation period of 3 μs). Virtually no conduction takes place with an applied potential of -100 mV and ϵ of 50. In a simulation period of 5.5 μs, only one calcium ion crosses the channel, resulting in a current of 0.06 pA.

The diffusion coefficient of ions inside the channel can be estimated from molecular dynamics simulations. There are a number of such studies which indicate that the diffusion coefficient is significantly reduced from its bulk value inside narrow channels (Roux and Karplus, 1991; Lynden-Bell and Rasaiah, 1996; Smith and Sansom, 1997, 1999; Allen et al., 1999a, b, 2000b). Allen et al. (2000b) have carried out a systematic study of diffusion coefficients of K^+, Na^+, Ca^{2+}, and Cl^- ions in cylindrical channels with radii varying from 3 to 7 Å. Here we use their estimates as a guide and use 0.5 times the bulk diffusion coefficient for calcium ions in the channel chamber ($-25 < z < 7.5$ Å) and 0.1 times the bulk in the selectivity filter ($7.5 < z < 20$ Å). Corresponding values of 0.5 and 0.4 times the bulk value are used for sodium. The bulk values are used in the reservoirs for all ions.

In Fig. 4 we illustrate the sensitivity of the channel conductance on the choice of diffusion coefficient. Here the diffusion coefficient of calcium ions is systematically varied from 0.05 to 0.5 times its bulk value in the selectivity filter while it is kept at 0.5 times the bulk in the chamber, and the resulting current is plotted. Contrary to intuitive expectations from continuum theories, the current does not increase linearly with the diffusion coefficient but rather saturates as one approaches toward the bulk value. For example, at the chosen value of 0.1 times the bulk, the calcium current is suppressed by only a factor of 2 rather than 10. This happens because ions have to overcome a potential barrier to conduct, which causes saturation of current in the limit of high diffusion coefficients (ballistic limit). Thus, we expect

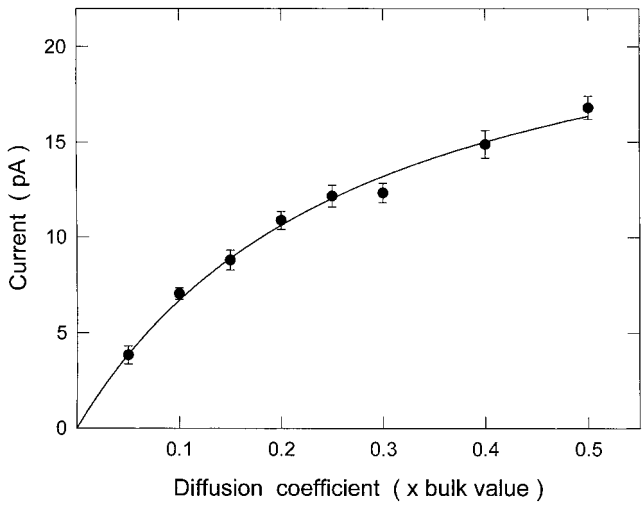

FIGURE 4 Dependence of calcium current on the ion diffusion coefficient in the narrow neck region of the channel (7.5 Å $< z <$ 20 Å) plotted as a fraction of its bulk value (0.79×10^{-9} m^2 s^{-1}). A concentration of 150 mM $CaCl_2$ is maintained in the reservoirs and a -200 mV driving force is used. Results are obtained from a 2 μs simulation period.

the results presented in this paper to be quite robust against variations in the diffusion coefficients.

Permeation of calcium and sodium ions

The ion-channel and ion-ion interactions hold the clue to understanding ion permeation mechanisms in channels. Therefore, we first present a detailed study of multi-ion potential energy profiles in the model channel to gain some useful insights. A quantitative description of ion permeation that includes the effects of the thermal motion of ions and their interaction with water molecules requires a dynamic approach, which will be discussed in the following sections by performing BD simulations.

Energy profiles

The ion-channel interaction has basically two components: a repulsive force due to the induced charges on the protein boundary and the electrostatic interaction of the ion with charge residues and dipoles in the channel wall. The simple Coulomb interaction between two ions is modified in the channel environment because they also interact via the surface charges induced by each other. All these effects are properly taken into account by solving Poisson's equation with appropriate boundary conditions as mentioned in the Methods section.

For a single ion, a potential energy profile is constructed by calculating the potential energy of the ion held at a fixed z position far from the channel and then repeating these calculations at discrete (1 Å) steps as the ion approaches the channel. While the main pathway of ions in the channel is along the central axis, due to asymmetric placement of glutamates, an ion's equilibrium position could deviate from the central axis by ~1 Å near the selectivity filter. To take this effect into account, the ion is held fixed only in the z direction, but allowed to move in the x and y directions to ensure that it is equilibrated in the x-y plane. To construct multi-ion profiles, one or more ions are placed in the channel at equilibrium positions and the potential energy of another ion is calculated as it is brought into the channel in 1 Å steps. Before calculating the potential energy of this ion at each fixed position, the ions in the channel are always equilibrated so that the force on them is zero and the system energy is at a minimum. As in the single ion case, only the z position of the external ion is fixed, and it is allowed to equilibrate in the x-y plane. The profile constructed in this way is equivalent to the total electrostatic energy required to bring the charge on the ions from infinity in infinitesimal amounts. The method used in minimizing the energy is detailed elsewhere (Chung et al., 1999).

The profile for an ion moving across the channel with no fixed charges in the walls is shown in Fig. 5. An ion entering the channel meets a steeply rising potential barrier, which is proportional to the square of the ion charge. Thus

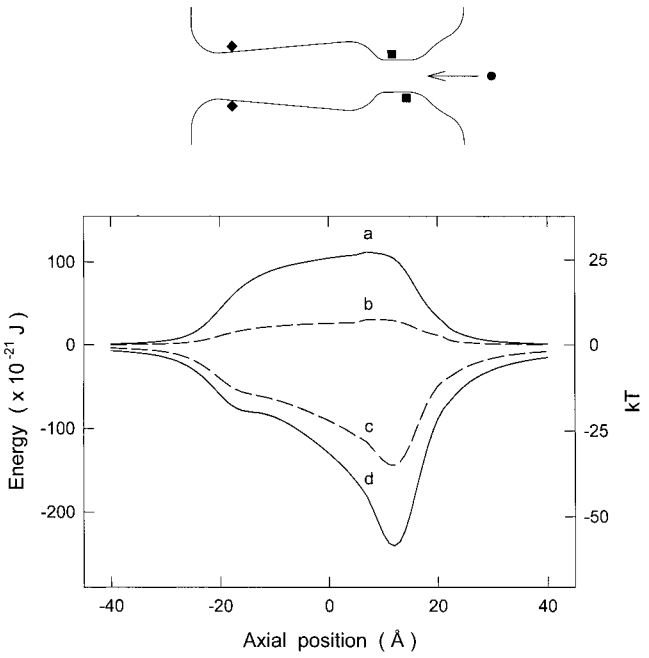

FIGURE 5 Electrostatic energy profile of an ion traversing the channel. The potential energy of an ion held at 1 Å intervals in the z direction but allowed to move to its minimum energy position in the x and y directions is plotted for a calcium ion (*solid line*, *a*) and a sodium ion (*dashed line*, *b*) in the absence of any fixed charges. When the glutamate groups and mouth dipoles are included, as shown in the inset, the profiles are replotted for calcium (*solid curve*, *d*) and sodium ions (*dashed line*, *c*). No applied potential is used. We note that 1 kT = 4.11×10^{-21} J.

the barrier height for calcium ions (28 kT, *solid curve labeled a*) is four times larger than sodium ions (7 kT, *dashed curve labeled b*). When the ring of four mouth dipoles and four glutamate charges are included in the model, this barrier is turned into a deep well. Again this well is deeper for divalent ions (58 kT, *solid curve labeled d*) than for monovalent ions (36 kT, *dashed curve labeled c*), though the difference is much less pronounced because ion-charge residue interaction is proportional to the ion charge (the energy difference between *a* and *d* is exactly twice that between *b* and *c*). For both types of ions, the well is deep enough so that a single ion would be permanently trapped in the selectivity filter.

Once an ion has entered the energy well, a second ion will see a very different profile, altered by the presence of the first. The profile seen by a second calcium ion when a first ion is in the energy well under a driving potential of −100 mV is shown in Fig. 6. The curve on the right (*dashed*) shows the potential energy of the second ion as it approaches the channel from the right, while the one on the left (*solid*) shows the same when the first ion moves out of the channel to the left. Clearly, both ions can still reside in local energy minima indicated by the arrows in the figure. The ion in the left well faces an energy barrier of ~4.7 kT, which it can surmount as a result of their random motions

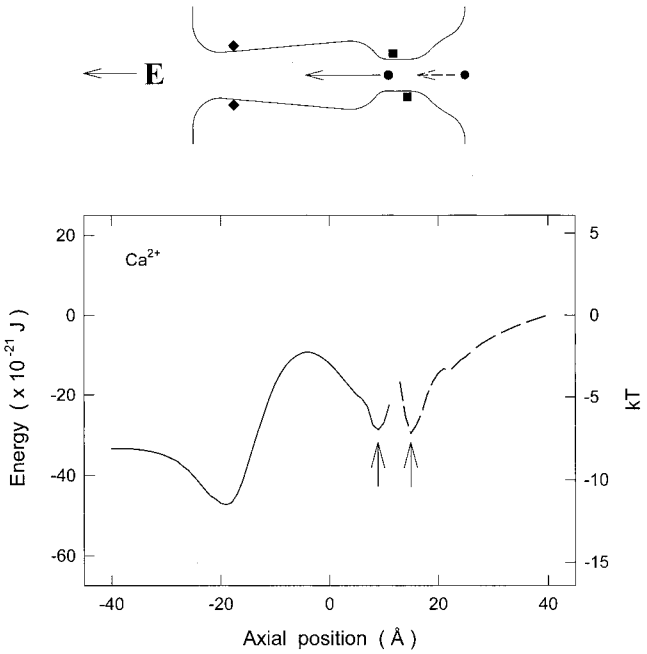

FIGURE 6 Electrostatic energy profiles with two calcium ions in the channel under a −100 mV driving force. The potential energy of a calcium ion entering the channel is calculated at 1 Å intervals along the *z* axis while another calcium ion is resident in the filter (*dashed curve*). Similarly, the potential energy encountered by the left-hand calcium ion as it attempts to cross-the channel is calculated at 1 Å intervals (*solid curve*). The second ion is allowed to move to its minimum energy position in the narrow channel neck in both cases. The equilibrium positions of the two calcium ions in the channel are indicated by the arrows. It should be noted that these are two distinct curves and the driving potential cannot be calculated from the total energy drop from right to left.

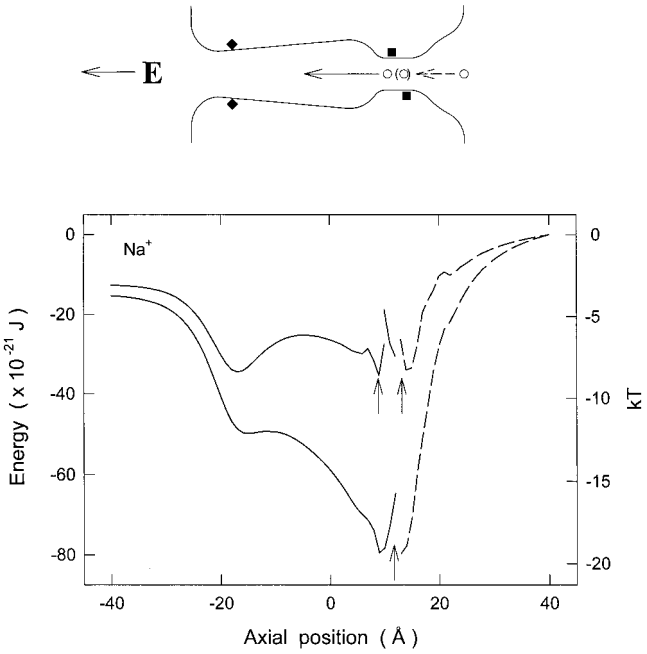

FIGURE 7 The energy profiles as in Fig. 6 except for a sodium ion with one (*lower curves*) or two (*upper curves*) other sodium ions in the channel neck. An applied potential of −100 mV is used. The equilibrium positions of the resident sodium ion(s) when the test ion is in the reservoir are indicated by the upward arrows.

and the mutual Coulomb repulsion. Once this happens, the ion on the left will move toward the interior mouth of the channel under a steep potential gradient. When the channel is occupied by two calcium ions, a third ion meets a very steep barrier, preventing its entry into the channel. The above study of multi-ion potential energy profiles thus indicates that the conduction of divalent ions is most likely to be a two-ion process.

For monovalent ions a different picture emerges. The well is in fact deep enough (20 kT) to hold two ions in a stable configuration at $z = 9$ and 13 Å, as indicated by the lower curves in Fig. 7. The two disjointed curves again correspond to the second ion being brought into the channel from the right (*dashed*) and the first exiting to the left (*solid*), respectively. In the absence of divalent ions, two monovalent ions are most likely to be found at these positions. When two monovalent ions are in the channel, the profile seen by a third ion is also shown in Fig. 7 (*upper curves*). In this case there is no longer a large potential well in the selectivity filter, and only a very small energy barrier (1 kT) preventing the left-most ion in the filter moving to the small well at the interior region created by the mouth dipoles. So the conduction of monovalent ions is expected to be a three-ion process, and because they face a smaller barrier, their permeation rate should be much higher than the divalent ions.

Current-voltage relationships

We study the conductance properties of calcium and sodium ions under various conditions by performing BD simulations. The current-voltage relationships shown in Fig. 8, *A* and *B* are obtained using symmetrical solutions of 150 mM $CaCl_2$ or 150 mM NaCl, respectively, and are fitted by the solid lines. Because the calcium current is so small at low applied potentials, it takes exorbitant amounts of simulation time to gain reliable statistics. For this reason values lower than +80 mV and −60 mV are not shown. The current-voltage relationship for the sodium current is fairly linear through the origin, although it does show some degree of nonlinearity at large applied voltages. In contrast, the calcium current deviates noticeably from an ohmic relationship as the applied potential is increased beyond ±100 mV. This superlinearity is a result of the large energy barrier in the channel, which presents less of an impediment to ion movement as the driving potential is increased (Chung et al., 1998). In both relationships there is a small asymmetry between the inward and outward currents. The current-voltage relationships obtained experimentally from L-type calcium channels appear to exhibit less asymmetry for both sodium and calcium ions (Rosenberg et al., 1986; Rosen-

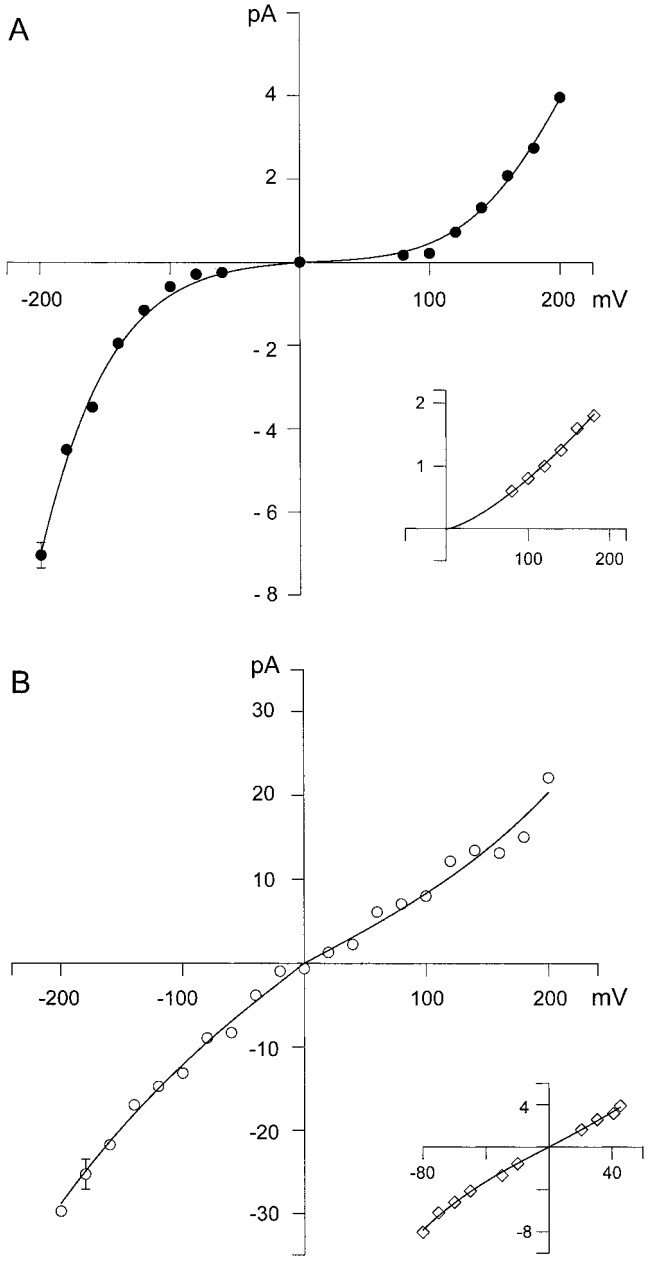

FIGURE 8 Current-voltage relationships. The magnitude of the current passing through the channel with a symmetric solution of (*A*) 150 mM $CaCl_2$ and (*B*) 150 mM NaCl in both reservoirs is plotted against the strength of the driving potential. The experimental results of Rosenberg and Chen (1991) in similar conditions are shown in the insets for comparison. A simulation period of 4 to 8 μs is used for calcium and 0.5 μs for sodium.

berg and Chen, 1991). We find from BD simulations that the symmetry of the calcium current depends crucially on the position and strength of the mouth dipoles. Thus any discrepancy between the experimental findings and the results of our simulations can be improved by adjusting these. With less charge on the dipoles the outward current becomes greater and the inward current smaller (see Fig. 3 *B*). Also, moving the dipoles closer to the interior mouth of the channel produces greater rectification, the inward current becoming much larger than the outward.

At -120 mV and with 150 mM solution, the inward currents for calcium and sodium are, respectively, 1.2 ± 0.2 pA and 14.7 ± 1.6 pA, giving the respective conductance values of 9.7 pS and 122 pS. These values are fairly close to the experimentally determined values of 8–9 pS for calcium with 100–110 mM solution and 85–90 pS for sodium in 150–200 mM solution (Hess et al., 1986; Rosenberg and Chen, 1991, Nilius et al., 1985). The superlinearity seen at large applied potentials has been observed in the *I-V* curves with symmetric solutions (Rosenberg and Chen, 1991), which are reproduced for calcium and sodium in the insets of Fig. 8, *A* and *B*.

Ions in the channel

The average distribution of ions in the channel for calcium and sodium ions under a -200 mV applied voltage is shown in Fig. 9, *A* and *B*, respectively. To find the average number of ions in each section of the channel, we divide it into 30 layers of thickness 1.6 Å as indicated in the inset, and compute the average number of ions in each layer throughout the simulation. For calcium ions, there are on average 1.9 ions in the channel, occupying the narrow selectivity filter most of the time. The ion distribution shows two clear peaks, indicating where the ions are most likely to be found at each end of the filter. Again, this supports the conclusion that calcium conduction requires multiple ions. For sodium there are on average 3.1 ions in the channel, and again the ions are most likely to be found in the narrow section. Sodium ions are more likely to occupy the interior end of the channel than the calcium ions, which can be easily understood in terms of the two- and three-ion profiles in Figs. 6 and 7, respectively.

Our BD simulations support the conjectures derived from the potential energy profiles, that conduction is achieved by the interaction between multiple ions in the channel, and that the channel is always occupied by one or more ions. For 150 mM $CaCl_2$ or 150 mM NaCl at -200 mV, the relative time the narrow section of the channel ($4 < z < 18.5$ Å) is occupied by one or more ions is shown in Table 2. That the filter is so often multiply occupied by calcium suggests that the time taken for one of the ions to move out of the filter, over the energy barrier toward the interior mouth, is one of the rate-limiting steps. This is shown more conclusively below. For sodium the filter is again occupied most commonly by two ions, suggesting that once a third ion enters conduction happens quite quickly. The different times between when an ion enters the channel and an ion traverses it for calcium and sodium reflects the different energy barriers presented in each case: sodium conducts much more quickly as it sees a much lower barrier.

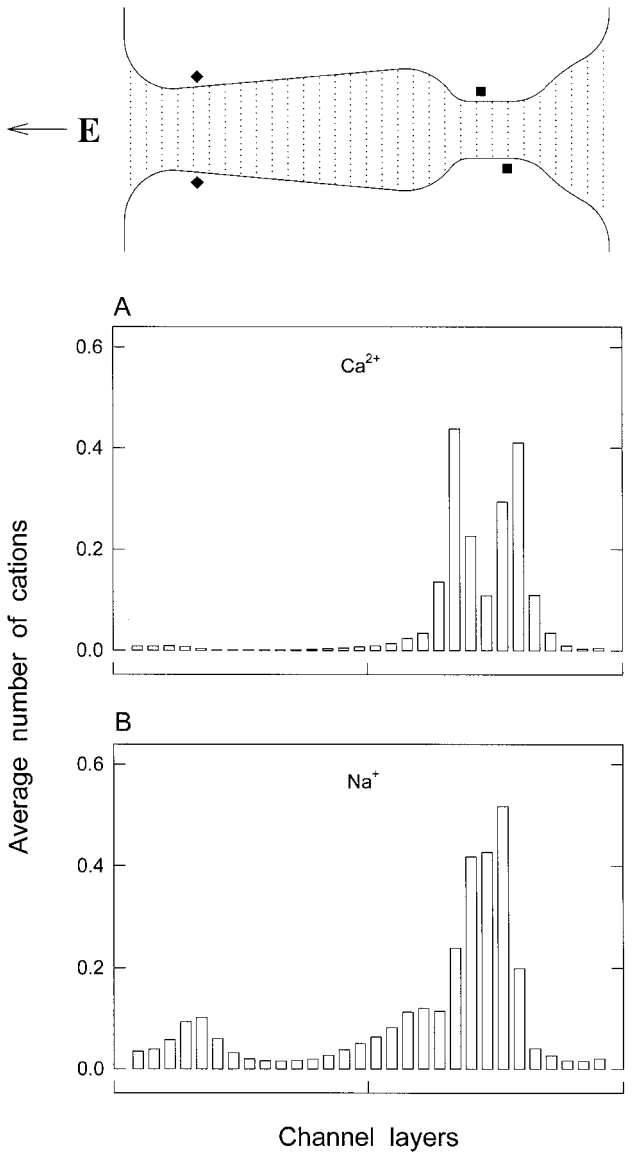

FIGURE 9 Average number of ions in the channel with an applied potential of −200 mV. The channel is divided into 30 sections, as shown in the inset, and the average number of ions in each calculated over a simulation period (0.5 μs) with (*A*) 150 mM $CaCl_2$ and (*B*) 150 mM NaCl in the reservoirs.

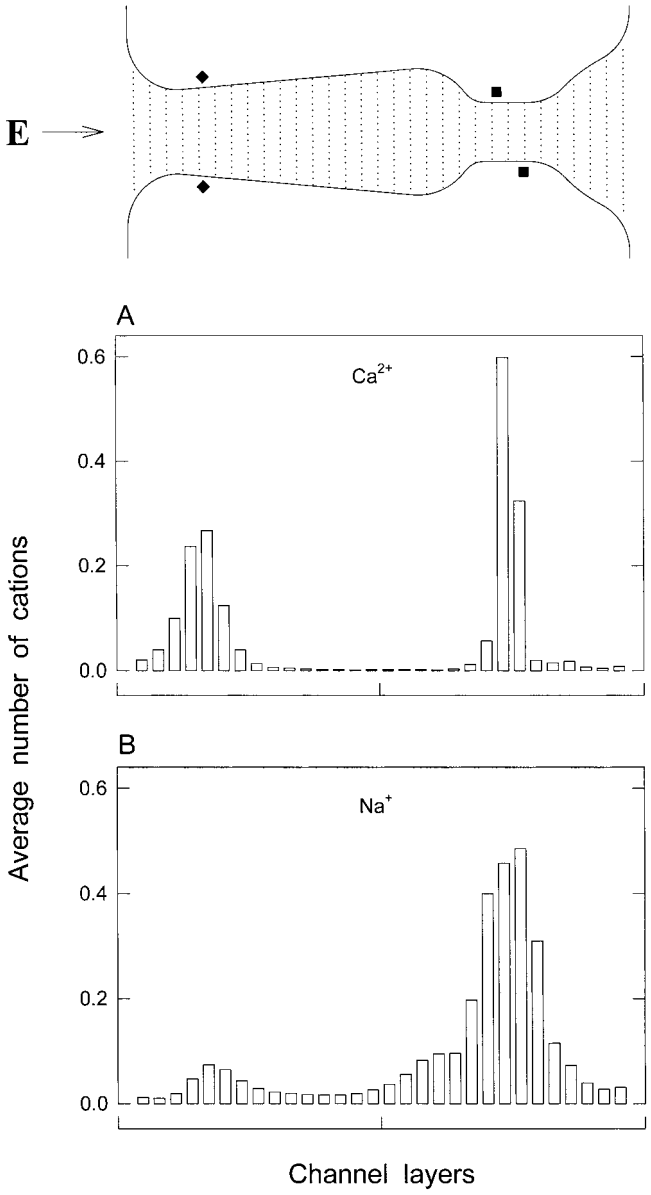

FIGURE 10 Average number of ions in the channel as in Fig. 9 except with an applied potential of +200 mV with (*A*) 150 mM $CaCl_2$ and (*B*) 150 mM NaCl in the reservoirs.

Under a +200 mV driving force producing an outward current the distribution of ions in the channel is very different, as is shown for calcium and sodium in Fig. 10, *A* and *B*. With 150 mM $CaCl_2$ in the reservoirs there are still on average 1.9 calcium ions in the channel, but rather than being predominantly located in the narrow neck of the channel, as was the case in an inward current, the ions are now almost equally likely to be found near the internal channel mouth as in the narrow filter. Indeed, the region near the internal mouth is occupied 85% of the time. The filter is always occupied, but, in contrast to the situation with an inward current, usually by only one ion (95% of the time). For sodium, the distribution of ions in the channel is very similar under either a −200 or +200 mV driving potential. As the energy barriers in the channel are small for

TABLE 2 Relative time selectivity filter is occupied by one, two, or three ions in 150 mM $CaCl_2$ or 150 mM NaCl

	No. ions in filter		
	1	2	3
Ca^{2+}	26%	74%	0%
Na^+	5%	77%	18%

sodium, the effect of the driving potential on the barriers does not significantly alter where ions are likely to be found.

To demonstrate more explicitly the rate-limiting steps for inward and outward calcium currents, we show in Fig. 11 the time taken for different permeation events. Fig. 11 *A* shows the energy profile presented to a calcium ion as in Fig. 6, except under a −200 mV driving potential. The height of the central barrier, V_B, is 2.9 kT. Given that the narrow section of the channel is always occupied, the time for a conduction event can be broken into two parts: τ_1, the time for a second calcium ion to enter the filter from the reservoir; and τ_2, the time for one of the ions in the filter to move across the central energy barrier once the second ion has entered, as indicated in the figure. From a conditional probability analysis of the ion trajectories in our BD simulations, we find that τ_2 takes an average of 33 ns, or 74% of the average conduction time of 45 ns, making it the rate-limiting step. The time for the second calcium ion to enter, τ_1, takes most of the remaining time (11 ns), indicating that once an ion crosses the central barrier it exits the channel almost instantaneously. This can also be seen in Fig. 9 *A*, which indicates that calcium ions rarely occupy the left-hand end of the channel. That the time spent waiting for one of the ions to cross the center of the channel is the rate-limiting step for inward currents raises the question of whether an ion moves across the barrier by its own thermal motion and the Coulomb repulsion of the second calcium ion, or whether it requires additional repulsion from a third ion entering the channel vestibule. A conditional probability analysis of how many ions are in the right-hand half of the channel ($0 < z < 25$ Å) while the innermost calcium ion is crossing the central barrier ($-10 < z < 0$ Å) shows that 99% of the time there is only one ion, and so the entry of a third ion into the channel is not required for calcium transit.

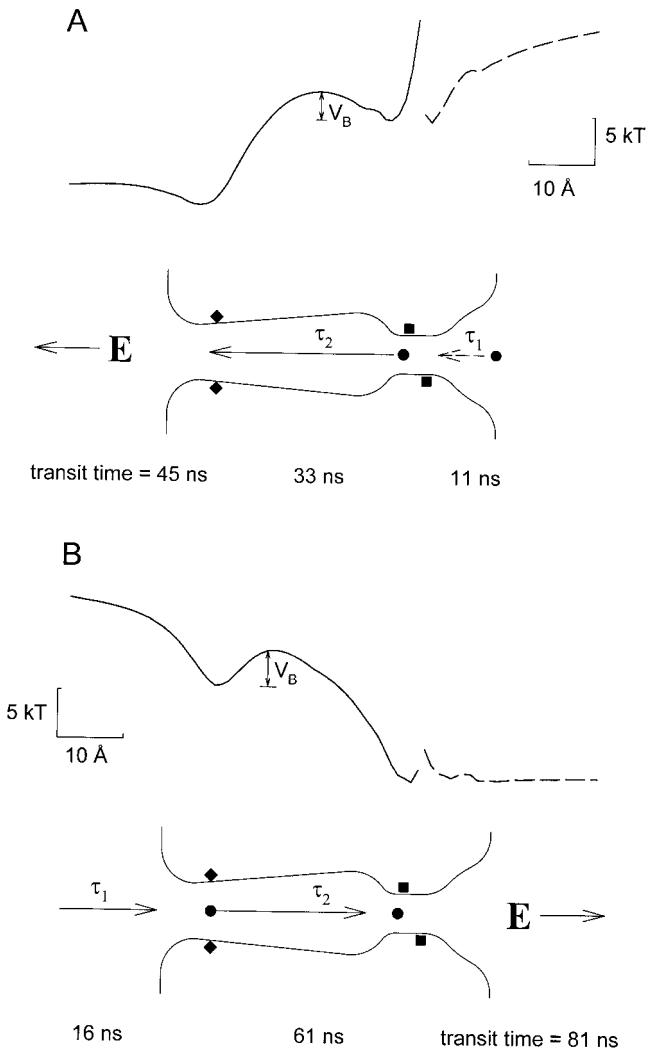

FIGURE 11 Rate-limiting steps for ion permeation. The energy profile presented to a calcium ion as in Fig. 6 and the main time-consuming steps for ion permeation are shown for (*A*) a −200 mV and (*B*) a +200 mV driving potential. In *A* the ions permeate from right to left and meet a central energy barrier $V_B = 2.9$ kT. In *B* the ions permeate in the opposite direction and meet a barrier of 3.7 kT. The time taken for a second ion to enter the channel, τ_1, and the time for an ion to cross the central barrier, τ_2, are indicated.

A similar analysis is shown for a +200 mV driving potential creating an outward current in Fig. 11 *B*. The conduction process is divided into the time for an ion to enter the left-hand end of the channel, τ_1, and the time for it to move across the central energy barrier ($V_B = 3.7$ kT) into the filter, τ_2, as indicated. Again, the rate-limiting step is the time to climb the central barrier, τ_2, which takes an average of 61 ns, accounting for 85% of the total conduction time (81 ns). The time spent waiting for an ion to enter the internal mouth of the channel accounts for most of the remaining time (16 ns), indicating that once two ions enter the filter, one quickly exits. This is clearly explained by examining the energy profile, which shows that there is virtually no barrier preventing this external exit.

Because climbing over the central barrier is the rate-limiting step in calcium permeation, calcium conductance will depend crucially on the barrier height. The height of the barrier, V_B, decreases fairly linearly for both inward and outward currents as the driving potential is increased, which, not surprisingly, results in larger currents. However, this does not mean that the current will also vary linearly, as can be seen in the current-voltage curves (Fig. 8).

Conductance-concentration relationships

If the transport of ions is dependent on two processes, one of which depends on concentration (access to the channel) and one which does not (permeation in the channel), then we expect the current I to eventually saturate with increasing ion concentration c, leading to a current-concentration relationship of the Michaelis-Menten form (Chung et al., 1999):

$$I = \frac{I_{max}}{1 + K_s/c}. \quad (6)$$

Here I_{max} denotes the saturation current and K_s the half-maximum concentration.

The current-concentration relationship found from BD simulations indeed has this form and is in close agreement with the experimentally observed shape (Hess et al., 1986; Ganitkevich and Isenberg, 1990). In Fig. 12 *A* the current-concentration relationships obtained from BD simulations (*filled circles*) are compared to the experimental results of Hess et al. (1986) (*diamonds* and *dotted line*). The BD data have been fitted using Eq. 6 (*solid line*) with a maximum current $I_{max} = 7.5$ pA and point of half-maximum $K_s = 13.9 \pm 2.5$ mM. This compares well with the K_s value of 13.9 mM quoted by Hess et al. (1986). The different scales in the figure arise as a higher applied potential is used for the BD simulations as required to obtain reliable statistics with a limited amount of computer time.

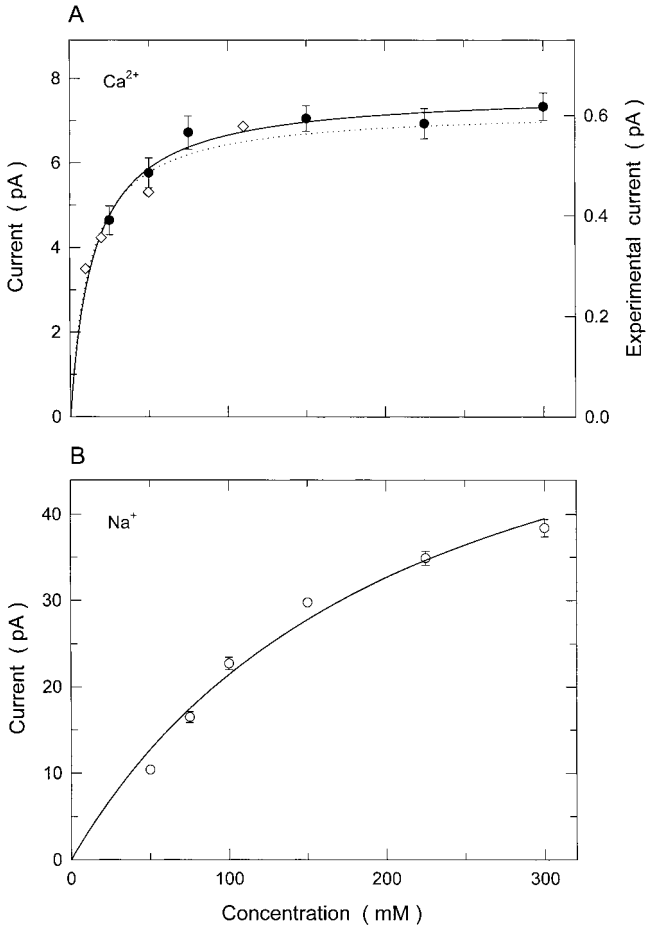

FIGURE 12 Current-concentration relationships. The current obtained with symmetrical solutions of varying concentrations of (*A*) $CaCl_2$ (*filled circles*) and (*B*) NaCl (*open circles*) in the reservoirs. An applied field of −200 mV is used and the data points are fitted by the solid line using Eq. 9. In *A* the experimental data of Hess et al. (1986) are shown by the open diamonds and dashed line for comparison. Note that the different scales on the simulation and experimental results are largely due to the different applied potentials in each case. For the BD results a simulation period of 4–8 μs and 0.5 μs are used for calcium and sodium, respectively.

The current-concentration relationship found with BD simulations for sodium has a similar shape but saturates much more slowly, as can be seen in Fig. 12 *B*. Again, this is fitted by a Michaelis-Menten equation with the value $I_{max} = 71$ pA and $K_s = 240$ mM. In both plots, a driving force of −200 mV is used.

Mixtures of calcium and sodium ions

It is important to see whether our model channel can account for experimental results with more than one ion species present. In particular we look at mixtures of calcium and sodium ions as an example of selectivity between monovalent and divalent ions. To answer such questions as the effect of each type of ion on the permeation of the other and the competition between different types of ions to access the selectivity filter, we again first consider potential energy profiles for mixed ions and then carry out BD simulations.

Energy profiles for mixed ions

First we look at the energy profiles with a mixture of calcium and sodium ions to gain an intuitive picture of how the presence of calcium ions may affect the permeation of sodium ions. We construct the energy profiles shown in Fig. 13 for a sodium and a calcium ion entering a channel occupied by an ion of the other species so that we can compute the energy required to push a resident calcium ion out of the channel. In this and the following figures, a potential of −100 mV is applied. The profile on the right between $z = 14-40$ Å (*dashed line*) shows the potential energy of a sodium ion as it is moved in 1 Å steps from the reservoir, while the resident calcium ion is allowed to adjust its position so as to minimize the total energy of the system. The initial position of the calcium ion is indicated as a filled circle in the inset and the positions of the sodium ion approaching from the reservoir toward the calcium ion are indicated by the open circle. The profile on the left (*solid line*) represents the energy barrier seen by the calcium ion as it moves out toward the intracellular space in 1 Å steps while the sodium ion is allowed to adjust its position so as to minimize the total energy of the system. Not surprisingly, the channel can easily hold a calcium and a sodium ion in stable equilibrium. The difference from the two calcium ion case (Fig. 6) is that the barrier faced by the calcium ion on the left is increased from 5 to 16 kT in the present case, which is insurmountable. Clearly, the Coulomb repulsion provided by a sodium ion is inadequate for ejecting the resident calcium ion from the selectivity filter.

If another sodium ion is brought in from the extracellular reservoir while a calcium and a sodium ion are resident on the left and right sides of the selectivity filter, respectively, it meets a steeply rising Coulomb barrier. In fact, unlike all the previous cases shown in Figs. 6, 7, and 13, there is no

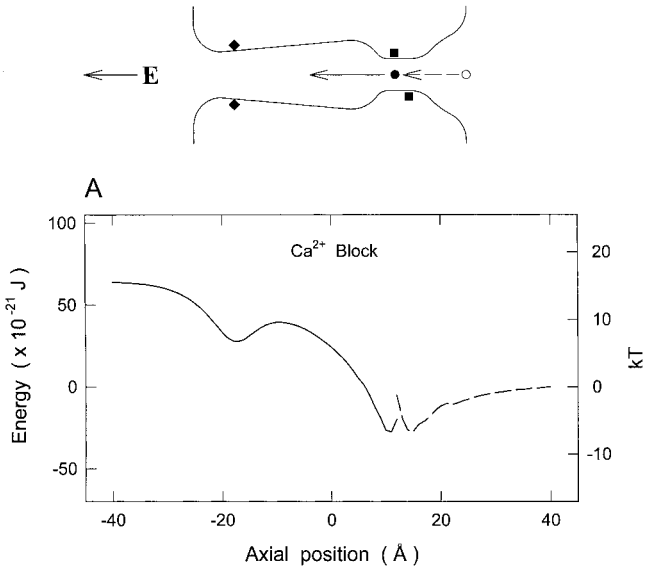

FIGURE 13 Energy profiles indicating calcium block. The right curve (*dashed line*) shows the potential energy of a sodium ion given that there is a calcium ion in the filter as indicated in the inset. The left curve (*solid line*) shows the potential energy of a calcium ion given that there is a sodium ion in the filter. The energies are calculated at 1 Å intervals as in Fig. 5 under a −100 mV driving potential.

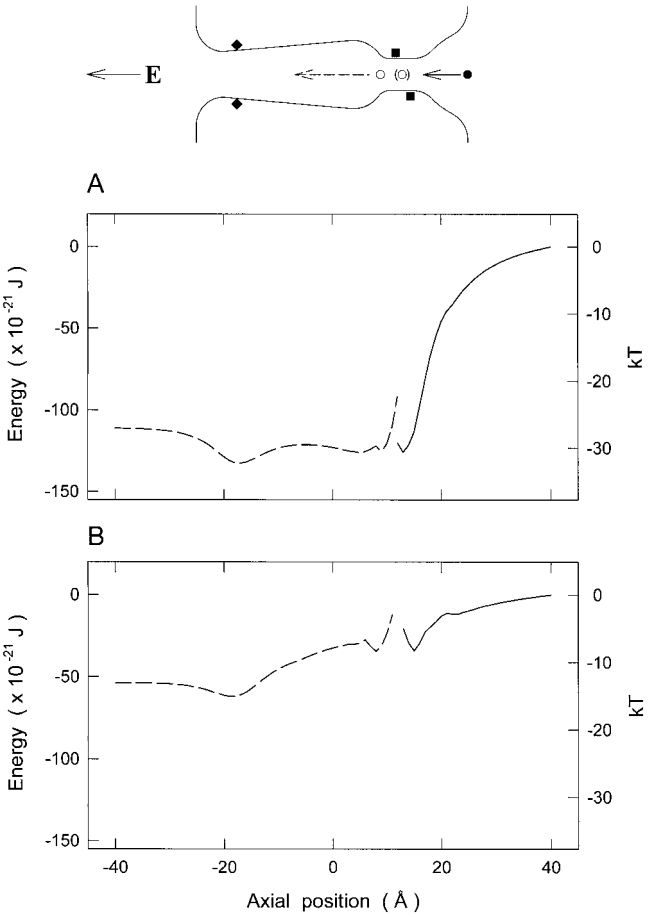

FIGURE 14 Energy profiles as in Fig. 13 except with a calcium ion on the right side of either (*A*) one, or (*B*) two sodium ions as shown in the inset.

stable equilibrium for one calcium and two sodium ions in the channel. The Coulomb barrier prevents the second sodium ion from moving toward the channel interior so that it is unable to dislodge the calcium ion from its minimum energy position. Even if a second sodium ion enters the exterior mouth through random motions, this will be a temporary event as it will be ejected quickly under the strong Coulomb repulsion from the resident ions. Thus, we expect from the study of the energy profiles that once a divalent ion enters the selectivity filter of the channel, it will permanently block the passage of monovalent ions.

We next examine whether the presence of one or more sodium ions in the channel is likely to block the passage of calcium ions. As before, we place one sodium ion in the selectivity filter and examine the profile encountered by a calcium ion as it enters from the right (*solid line* in Fig. 14 *A*), and the profile encountered by a sodium ion as it attempts to traverse the channel under the influence of the electric field and the repulsive Coulomb force exerted by the calcium ion (*dashed line* in Fig. 14 *A*). The calcium ion sees a large potential drop attracting it into the channel and there is only a small barrier preventing the sodium ion from exiting the channel. Thus, a single sodium ion in the filter will not prevent a calcium ion entering. The same conclusion is reached with two sodium ions in the channel (Fig. 14 *B*). The calcium ion still sees an attractive potential (*solid line*) and will easily access the channel. The profile on the left (*dashed line*) shows the potential energy of the inner sodium ion as it attempts to exit the channel to the intracellular side. As this is a well rather than a barrier, the left-most sodium ion will be easily pushed out once a calcium ion enters the channel. Thus, monovalent ions cannot prevent divalent ions from crossing the channel. Experimentally, however, a high sodium concentration attenuates the calcium current. Explanation of this feature requires BD simulations and, as shown in a later section, the experimental findings are replicated in our model.

Current-voltage relationship in mixed solutions

BD simulations, carried out with a mixture of calcium and sodium ions in the reservoir, confirm the block of sodium current by calcium ions conjectured above from the inspection of the potential energy profiles. Once a calcium ion enters the narrow section of the channel it prevents sodium ions from crossing the channel, but not vice versa. The current-voltage relationship obtained in the presence of a combination of calcium and sodium ions is markedly different from that obtained from a solution containing only one cationic species. Fig. 15 shows the magnitude of the

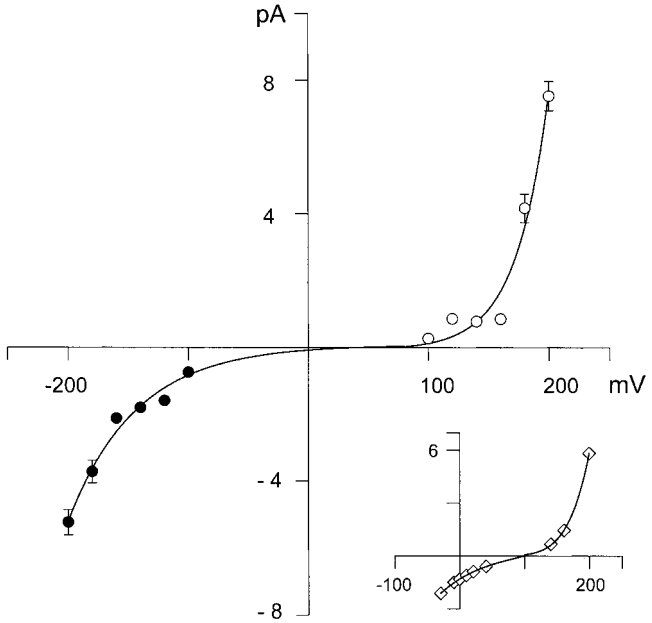

FIGURE 15 Asymmetric *I-V* curve with a mixture of Ca^{2+} and Na^{+} ions. The calcium (*filled circles*) and sodium (*open circles*) current passing through the channel is calculated at various applied voltages with 100 mM $CaCl_2$ and 50 mM NaCl in the external reservoir and 50 mM NaCl in the internal one. Data points represent the results of 2.5–7.5 μs simulations. The experimental data of Rosenberg et al. (1986) with a similar mixture of Ba^{2+} and Li^{+} ions are shown in the inset for comparison.

current as the voltage is varied with 100 mM $CaCl_2$ and 50 mM NaCl in the external reservoir, and only 50 mM NaCl on the internal side. Again, we have not carried out simulations below $\pm$100 mV due to the large simulation times required to gain reliable statistics at low currents. Due to the asymmetric concentrations, the reversal potential is $\sim$50 mM. Below this point, the inward current is mostly carried by calcium ions as they block sodium permeation. The conductance value is $\sim$25% lower than that found for calcium alone. How the presence of sodium lowers the calcium current is discussed below. The external current, however, climbs rapidly above the reversal potential, reaching a larger value than the inward current as it is carried by more rapidly permeant monovalent ions. This outward monovalent current, however, displays a different shape to that seen for sodium alone, rising slowly at first and then very rapidly at higher potentials. The reason for this is that calcium ions on the external side of the channel still occasionally move against the driving potential and fall into the channel, blocking the monovalent current. At higher positive applied potentials, this no longer happens and the sodium current is not impeded.

The general shape of this graph agrees closely with that found experimentally in similar conditions by Rosenberg et al. (1986) which is represented in Fig. 15, *inset*. (Note that these experimental results are obtained using Ba^{2+} and Li^{+} ions, which have different conductance values from Ca^{2+} and Na^{+}.)

Mole fraction effect

Experimental studies of calcium channels have shown remarkable behavior in mixtures of monovalent and divalent ions. As the relative concentration of calcium to sodium is decreased, the conductance of the channel first decreases to a minimum and then increases again to a maximum when there is no calcium present (Almers et al., 1984). This so-called "anomalous mole fraction effect" has been a major subject of attention in calcium channel literature (see, for example, Tsien et al., 1987; Dang and McCleskey, 1998; Nonner and Eisenberg, 1998).

To investigate this behavior in our channel model we conduct BD simulations holding the sodium concentration fixed at 150 mM (8 ions in each reservoir) and measure the calcium and sodium currents in the channel at different calcium concentrations, as shown in Fig. 16 *A*. The calcium current is determined at higher concentrations ($\geq$37.5 mM) through BD simulations. As noted in the previous sections, sodium only conducts through the channel until it becomes blocked by a calcium ion. Thus, to calculate the sodium current we need only find how long it takes for a calcium ion to enter the channel and the rate at which sodium conducts before this. The time taken for a calcium ion to enter the channel is determined at 18 mM and above by repeatedly running BD simulations and calculating an average time for calcium entry. At low calcium concentrations, we can expect that sodium will conduct up until this point as if there were no calcium ions present.

This same technique, however, does not allow us to probe calcium concentrations lower than 18 mM, as we must have a very large reservoir to include a calcium ion. In such cases the BD simulations become cumbersome and impractical, as we also have to simulate the motion of a very large number of sodium and chloride ions. To obviate these problems, we extrapolate to lower concentrations using values at higher ones. We note that if our reservoir is larger than about two Debye lengths the effect of the channel and fixed charge environment will be totally screened out at the reservoir edges, allowing us to mimic lower concentrations by letting calcium ions randomly enter the reservoir as if in a larger bulk solution. In other words, the time for an ion to enter the finite reservoirs is inversely proportional to the calcium concentration. (For example, at a concentration of 2 mM we would expect the ion to be in the reservoir only one-tenth as long as at 20 mM.) Sodium only conducts before the channel becomes blocked by calcium or closes through some other gating mechanism. Thus, when the time taken for calcium block becomes larger than the mean open time of the channel, which is $\sim$1 ms for an L-type calcium channel (Hess et al., 1986; Hess, 1987), the sodium current saturates at its value in the absence of calcium. Although

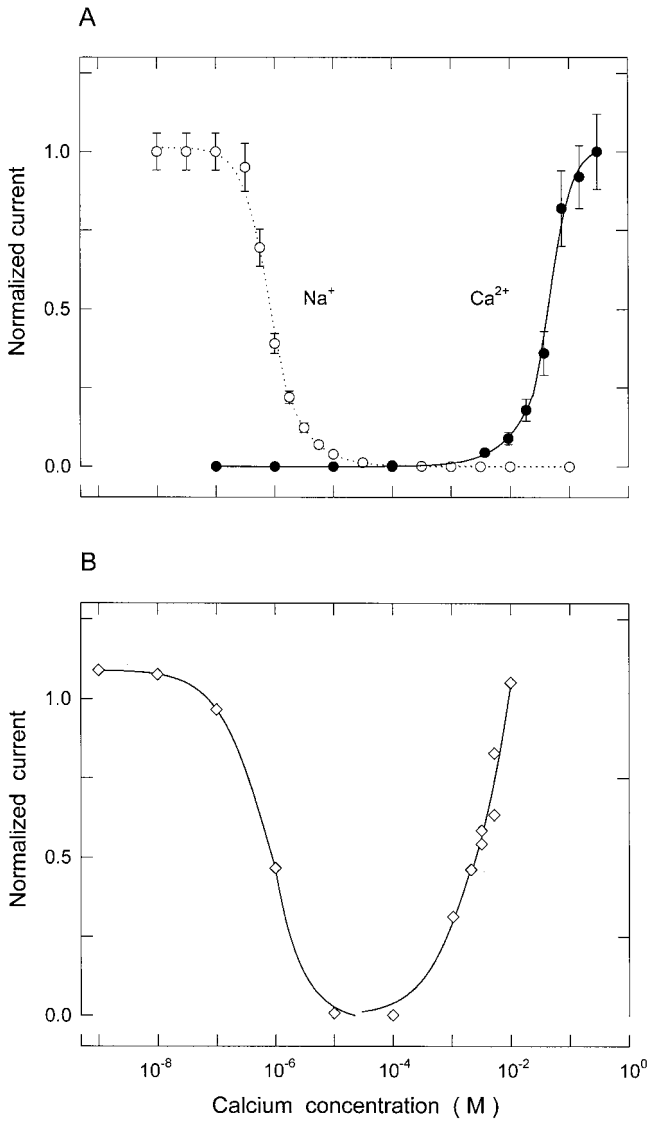

FIGURE 16 Mole fraction effect. (*A*) The Ca^{2+} (*filled circles*) and Na^{+} (*open circles*) currents across the channel determined with different symmetrical calcium concentrations in the reservoirs from BD simulations as described in the text. The sodium concentration is held fixed at 150 mM in both reservoirs and the applied voltage at −200 mV in all cases. (*B*) A representation of the experimental results of Almers et al. (1984) is shown for comparison. Calcium currents come from 2 to 3 μs simulation periods, sodium currents from the simulation of 35 blocking events.

extrapolating the time to block in this way determines the shape of the sodium current curve, the position of the half-maximum current is highly dependent on the time taken for the channel to block at higher concentrations. Thus, comparing this value with experimental data still provides an important test of our model.

The values of the calcium and sodium current at different calcium concentrations, normalized by the maximum value of each, are shown by the filled and open circles in Fig. 16 *A*, respectively. (It should be noted that the magnitude of the calcium current is significantly lower than that for sodium.) As the calcium concentration decreases the calcium current also decreases, as was the case in the concentration conductance curve, since it takes longer for a second calcium ion to enter the channel as required for conduction. With further reduction in calcium concentration, it takes longer for a calcium ion to enter and block the channel, meaning more sodium ions are able to pass through the channel before this occurs. Thus the sodium current keeps increasing until it saturates when the time to block reaches the mean open time of the channel.

The resulting picture is the well-known mole fraction effect. As the calcium concentration is decreased, the total current passing through the channel first decreases and then increases again. For comparison, the experimental results of Almers et al. (1984) are shown in Fig. 16 *B*. Our extrapolation from BD simulations predicts the half-maximal sodium current to occur at a calcium concentration of $\sim 8.6 \times 10^{-7}$ M, close to the experimentally determined value of $\sim 8.8 \times 10^{-7}$ M. Although we have held the sodium concentration at 150 mM throughout, the data points on the right-hand side of the experimental figure are obtained with no sodium present. As discussed below, the presence of sodium can attenuate the calcium current, therefore our values of calcium current can be expected to be lower than those in the experimental curve. Also, it is worth noting that the simulation data are normalized by the current at near-saturation value; the experimental data, however, are normalized by a lower value than this. If the saturation current were to be used in the experimental data, the normalized calcium current would be lower than shown.

Attenuation of calcium currents by sodium

We have seen that once a calcium ion enters the channel, it prevents sodium ions from permeating. A number of results suggest that the presence of monovalent ions can also slow the permeation of calcium ions. For example, at physiological concentrations of sodium and calcium, external sodium attenuates calcium current through the channel (Polo-Parada and Korn, 1997); in channels carrying outward lithium currents, high extracellular concentrations of lithium ions slow the rate at which calcium ions exit the pore, producing the so-called "lock-in effect" (Kuo and Hess, 1993b); finally, increasing the external concentration of lithium is found to slow the entry rate of external calcium ions into the pore (Kuo and Hess, 1993b). All of these results suggest that the external monovalent ions interfere with the entry and exit of calcium ions on the external side of the pore.

To examine the effect of external sodium ions in our model, we hold the calcium concentration in each reservoir fixed at 150 mM (8 ions in each reservoir) and vary the sodium concentration from 0 to 300 mM. Fig. 17 *A* shows the normalized channel current obtained by dividing the current by that in the absence of sodium. The BD simulation

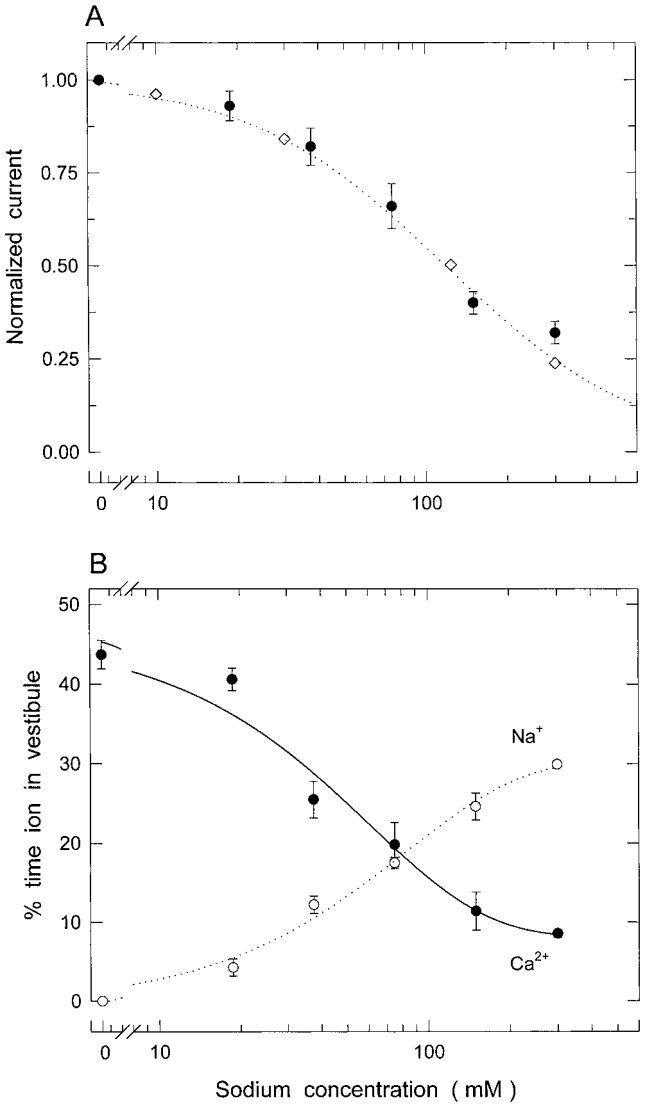

FIGURE 17 Attenuation by external sodium. (*A*) The normalized channel current, calculated by dividing by the value in the absence of sodium, is shown as the sodium concentration in the reservoirs is varied in BD simulations (*filled circles*). The calcium concentration is held fixed at 150 mM in both reservoirs throughout and a −200 mV driving potential is used. The experimental data and fit of Polo-Parada and Korn (1997) are shown by the open diamonds and dotted line for comparison. (*B*) The percentage of time that the external vestibule of the channel is occupied by Ca^{2+} (*filled circles*) or Na^{+} (*open circles*) given that there is a calcium ion in the channel neck for the simulations shown in *A*. A 3–4 μs simulation period is used.

results (*filled circles*) show that, as the sodium concentration is increased, the calcium current severely decreases. The BD data points are very close to the experimental results of Polo-Parada and Korn (1997), which are indicated by the open diamonds and fitted with the equation (*dotted line*)

$$Y = 1 - ([\mathrm{Na}]^k/IC_{50}^k + [\mathrm{Na}]^k), \qquad (7)$$

where $IC_{50} = 118.5$ mM and $k = 1.2$. Thus, the blocking of calcium current by external sodium is very well reproduced in this model.

It has been suggested that the block by external sodium is a consequence of calcium and sodium ions competing for the high-affinity site in the pore, and Dang and McCleskey (1998) take this effect to be evidence for a low-affinity site on the outside of the main high-affinity site. To understand the reason behind this blocking, we examine how an increase in the sodium concentration influences the calcium concentration near the external mouth of the channel. In Fig. 17 *B* we show the probability of finding a calcium ion (*filled circles*) or a sodium ion (*open circles*) in the external vestibule of the channel given that there is a calcium ion in the filter. In the absence of sodium ions in the electrolyte, the chance of finding a calcium ion in the vestibule while another one is in the filter is 44%. However, when sodium ions are introduced this probability drops rapidly. A sodium ion in the vestibule cannot push the calcium ion out of the filter, but it provides sufficient Coulomb repulsion to prevent other calcium ions from entering the vestibule, effectively stopping the conduction process. Due to its random motion, the sodium ion eventually leaves the vestibule and allows the other calcium ions to enter, but as can be seen in Fig. 17 *B* the presence of a sodium ion in the vestibule significantly decreases the chance of a calcium ion finding its way into the entrance of the channel. With a sodium concentration of 300 mM, a calcium ion enters the vestibule while another is in the filter only ~10% of the time. Thus the current is expected to be less than a quarter of its value in the absence of external sodium, consistent with the 75% attenuation observed in experiments. The above analysis suggests that the attenuation of channel current by external sodium is the result of competition between ions accessing the external vestibule of the channel rather than due to the presence of a specific low-affinity binding site.

Chloride ions play an important role in helping to alleviate the block by external sodium. Because the attenuation of current is a result of sodium ions inhabiting the channel vestibule and preventing calcium ions from entering, the calcium current will be strongly dependent on how long it takes for sodium ions to exit from the vestibule once they have entered. As seen in Fig. 13, a sodium ion, once inside the channel, faces a sizable barrier (7 kT) to move back to the external reservoir. This would be a very rare event if there were no assistance from counterions. When chloride ions are prevented from entering the vestibule (through an artificial block introduced into the BD simulations), the sodium ions attenuate the current much more effectively than when chloride ions are free to enter. As an example, with 150 mM calcium and 37.5 mM sodium (8 and 2 ions) in each reservoir, the current when the chloride ions are prevented from entering the vestibule is 3.2 ± 0.8 pA compared to 8.7 ± 0.8 pA when they are free to roam. This example highlights the role played by the counterions in

pulling the sodium ions out of the vestibule with their Coulomb attraction.

Mutation studies

Mutations of the glutamate residues have provided many useful insights into the binding and selectivity of the calcium channel. The replacement of one or more of the glutamate residues with neutral or positively charged residues severely lowers the conductance of the channel for divalent ions, and to a lesser extent for monovalent ions (Parent and Gopalakrishnan, 1995; Bahinski et al., 1997). Also, the block of monovalent currents by divalent ions is severely hampered, only arising at much higher divalent concentrations than for wild-type channels (Yang et al., 1993; Kim et al., 1993; Ellinor et al., 1995; Bahinski et al., 1997), giving evidence that the glutamate residues form a single binding zone leading to the high selectivity of the channel.

Here we attempt to replicate these experimental findings using our model calcium channel. In the BD simulations, we mimic the experimental site-directed mutagenesis by removing one of the charges representing the glutamate residues. With only three remaining glutamate residues in the channel, we find that the current is maximized when the charge on each amino acid is a full 1.6×10^{-19} C. That protonation should occur to a lesser degree in the mutated channel is plausible because there is less charge in the channel to attract and bind protons, and protonation is believed to be due to a cooperative effort of two or more glutamates (Chen et al., 1996; Morrill and MacKinnon, 1999; Chen and Tsien, 1997).

Examination of the potential energy profiles with three glutamate charges shows that the energy wells become less deep, so they are expected to be less effective in attracting cations. In Fig. 18 *A* we show how the selectivity of the channel for calcium over sodium, and the effectiveness of calcium block, diminish when the innermost (*squares*) or outermost (*triangles*) glutamate group is removed, compared to when all are present (*filled circles*). The plot shows the dependence of the sodium current on calcium concentration normalized by the maximum value in the same way as in Fig. 16 *A*. As noted earlier the values in this plot are extrapolated from values at higher concentrations. We find that the removal of one of the glutamate groups results in calcium ions taking longer on average to enter and block the channel, suggesting that sodium ions get more of a chance to permeate through the channel, and so it becomes less selective. When one of the central groups is removed we find the shift in selectivity is of similar range to the cases shown. For comparison we have shown some of the experimental data from Yang et al. (1993) in Fig. 18 *B*. These curves show the fractional lithium current passing through the channel as a function of calcium concentration and indicate the range of selectivity shift when one of the glutamate groups is replaced with glutamine. Our BD results show a shift in selectivity similar to that found experimentally, but the range of the effect is not as large. Naturally, a more accurate modeling of the channel is required to improve agreement with the experiment.

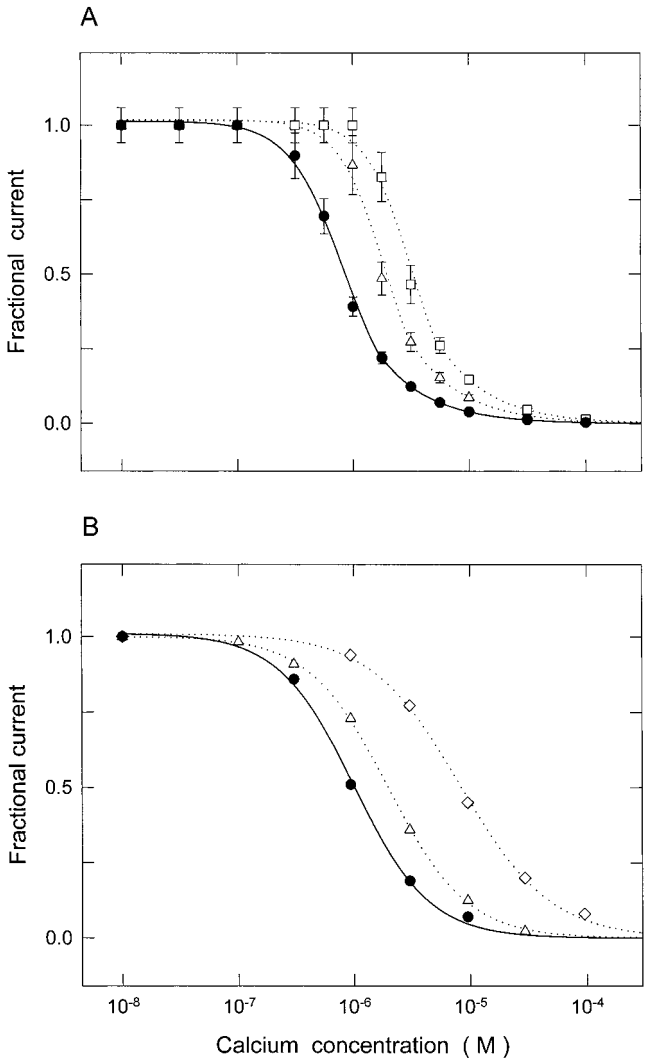

FIGURE 18 (*A*) The effect of removing glutamate charges on the channel selectivity in our model is shown by plotting the sodium current passing through the channel at different calcium concentrations with all four glutamate charges in place (*filled circles*), the outermost glutamate charge removed (*triangles*), and the innermost glutamate charge removed (*squares*); otherwise, all conditions are as in Fig. 16 *A*. Data points come from the simulation of 35 blocking events. (*B*) A selection of the experimental data with all glutamate residues in place (*filled circles*) and when two different residues are replaced with glutamine (*triangles* and *diamonds*) from Yang et al. (1993) is shown for comparison.

CONCLUSIONS

Although the crystal structure of the calcium channel is not yet known, we have constructed a model of the calcium channel using constraints derived from a number of experimental measurements. For the purposes of carrying out

electrostatic calculations and BD simulations, this model is a rigid and fixed structure. Most notably, the channel contains a narrow region with the glutamate residues near the extracellular end that forms the selectivity filter and is responsible for many of its distinctive characteristics. The narrowness of this section of the channel prevents ions from passing each other, making this a single file model, a point which is essential for explaining the mechanism of calcium block. The highly charged glutamate groups create a deep potential well that attracts surrounding cations. Once an ion enters this region of the channel, the depth of this well makes it difficult for that ion to exit on its own. Thus, this section of the channel is permanently occupied and roughly corresponds to the binding site discussed in reaction rate models. The model shape also has a wide but short external vestibule responsible for the attenuation of calcium current by sodium ions. The remainder of the channel is made up of a wider central chamber converging to a narrower intracellular entrance, similar in shape to the recently crystallized KcsA potassium channel.

Despite several gross simplifications in its construction, our rigid model is able to give a very clear explanation for many of the observed properties of calcium channels and reproduces a number of experimental results. We have demonstrated that permeation is a multi-ion process (2 ions for calcium and 3 ions for sodium), and the Coulomb repulsion plays a crucial role in this process. Selectivity arises from the strong electrostatic attraction of a divalent ion in the energy well and the inability of a monovalent ion to push it out. The conductance values of calcium and sodium ions closely match the experimental data. Similarly, the current-voltage and current-concentration curves deduced from BD simulations bear close resemblances to those measured experimentally. We also offer plausible physical explanations for the anomalous mole fraction effect between calcium and sodium, and the results obtained from studies involving site-directed mutagenesis.

There are several fine details of the channel that stochastic dynamics simulations cannot unravel. Among these are the permeation or selectivity sequence among monovalent and divalent ions and the blockage of the channel by certain divalent ions, such as nickel and zinc. The physical mechanisms underlying these phenomena may be elucidated by using molecular dynamics simulations, or if that fails, through ab initio methods. Because these methods are computationally very intensive, they cannot be used directly in modeling conductance of ion channels. Thus, for theoretical studies of ion channels, we need to develop a computational approach that combines molecular and BD simulations, the former explaining microscopic properties of the channel and providing parameters that can be used in the latter to explain its conductance and other related properties.

This work was supported by grants from the Australian Research Council and the National Health and Medical Research Council of Australia. The calculations upon which this work is based were carried out using the Fujitsu VPP-300 and the Linux alpha cluster of the ANU Supercomputer Facility.

REFERENCES

Allen, T. W., A. Bliznyuk, A. P. Rendell, S. Kuyucak, and S. H. Chung. 2000a. The potassium channel: structure, selectivity and diffusion. *J. Chem. Phys.* 112:8191–8204.

Allen, T. W., S. Kuyucak, and S. H. Chung. 1999a. Molecular dynamics study of the KcsA potassium channel. *Biophys. J.* 77:2502–2516.

Allen, T. W., S. Kuyucak, and S. H. Chung. 1999b. The effect of hydrophobic and hydrophilic channel walls on the structure and diffusion of water and ions. *J. Chem. Phys.* 111:7985–7999.

Allen, T. W., S. Kuyucak, and S. H. Chung. 2000b. Molecular dynamics estimates of ion diffusion in model hydrophobic and the KcsA potassium channels. *Biophys. Chem.* 86:1–14.

Almers, W., and E. W. McCleskey. 1984. Non-selective conductance in calcium channels of frog muscle: calcium selectivity in a single file pore. *J. Physiol.* 353:585–608.

Almers, W., E. W. McCleskey, and P. T. Palade. 1984. A non-selective cation conductance in frog muscle membrane blocked by micromolar external calcium ions. *J. Physiol.* 353:565–583.

Armstrong, C. M., and J. Neyton. 1991. Ion permeation through calcium channels: a one site model. *Ann. NY Acad. Sci.* 635:18–25.

Bahinski, A., A. Yatani, G. Mikala, S. Tang, S. Yamamoto, and A. Schwartz. 1997. Charged amino acids near the pore entrance influence ion-conduction of a human L-type cardiac calcium channel. *Mol. Cell. Biochem.* 166:125–134.

Bek, S., and E. Jakobsson. 1994. Brownian dynamics study of a multiply occupied cation channel: application to understanding permeation in potassium channel. *Biophys. J.* 66:1028–1038.

Bezanilla, F., and C. M. Armstrong. 1972. Negative conductance caused by entry of sodium and cesium ions into the potassium channels of squid giant axons. *J. Gen. Physiol.* 60:588–608.

Chen, X. H., I. Bezprozvanny, and R. W. Tsien. 1996. Molecular basis of proton block of L-type Ca^{2+} channels. *J. Gen. Physiol.* 108:363–374.

Chen, X. H., and R. W. Tsien. 1997. Aspartate substitutions establish the concerted action of p-region glutamates in repeats I and III in forming the protonation site of L-type Ca^{2+} channels. *J. Biol. Chem.* 272: 30002–30008.

Chung, S. H., T. W. Allen, M. Hoyles, and S. Kuyucak. 1999. Permeation of ions across the potassium channel: Brownian dynamics studies. *Biophys. J.* 77:2517–2533.

Chung, S. H., M. Hoyles, T. W. Allen, and S. Kuyucak. 1998. Study of ionic currents across a model membrane channel using Brownian dynamics. *Biophys. J.* 75:793–809.

Cooper, K. E., E. Jakobsson, and P. Wolynes. 1985. The theory of ion transport through membrane channels. *Prog. Biophys. Mol. Biol.* 46: 51–96.

Corry, B., S. Kuyucak, and S. H. Chung. 1999. Test of Poisson-Nernst-Planck theory in ion channels. *J. Gen. Physiol.* 114:597–599.

Corry, B., S. Kuyucak, and S. H. Chung. 2000a. Invalidity of continuum theories of electrolytes in nanopores. *Chem. Phys. Lett.* 320:35–41.

Corry, B., S. Kuyucak, and S. H. Chung. 2000b. Tests of continuum theories as models of ion channels. II. Poisson-Nernst-Planck theory versus Brownian dynamics. *Biophys. J.* 78:2364–2381.

Dang, T. X., and E. W. McCleskey. 1998. Ion channel selectivity through stepwise changes in binding affinity. *J. Gen. Physiol.* 111:185–193.

Doughty, S. W., F. E. Blaney, B. S. Orlek, and W. G. Richards. 1998. A molecular mechanism for toxin block in N-type calcium channels. *Protein Eng.* 11:95–99.

Doughty, S. W., F. E. Blaney, and W. G. Richards. 1995. Models of ion pores in N-type voltage gated calcium channels. *J. Mol. Graph.* 13: 342–348.

Doyle, D. A., J. M. Cabral, R. A. Pfuetzner, A. Kuo, J. M. Gulbis, S. L. Cohen, B. T. Chait, and R. MacKinnon. 1998. The structure of the

potassium channel: molecular basis of K^+ conduction and selectivity. *Science.* 280:69–77.

Ellinor, P. T., J. Yang, W. A. Sather, J. F. Zhang, and R. W. Tsien. 1995. Ca^{2+} channel selectivity at a single locus for high-affinity Ca^{2+} interactions. *Neuron.* 15:1121–1132.

Fukushima, A., and S. Hagiwara. 1985. Currents carried by monovalent cations through calcium channels in mouse neoplastic B lymphocytes. *J. Physiol.* 358:255–284.

Ganitkevich, V. Y., and G. Isenberg. 1990. Contribution of two types of calcium channels to membrane conductance of single myocytes from guinea-pig coronary artery. *J. Physiol.* 426:19–42.

Guàrdia, E., and J. A. Padró. 1996. On the influence of ionic charge on the mean force potential of ion pairs in water. *J. Chem. Phys.* 104: 7219–7222.

Guàrdia, E., R. Rey, and J. A. Padró. 1991a. Potential of mean force by constrained molecular dynamics: a sodium chloride ion-pair in water. *Chem. Phys.* 155:187–195.

Guàrdia, E., R. Rey, and J. A. Padró. 1991b. Na^+-Na^+ and Cl^--Cl^- ion pairs in water: mean force potentials by constrained molecular dynamics. *J. Chem. Phys.* 95:2823–2831.

Guàrdia, E., A. Robinson, and J. A. Padró. 1993. Mean force potential for the calcium-chloride ion pair in water. *J. Chem. Phys.* 99:4229–4230.

Guy, H. R., and S. R. Durell. 1995. Structural models of Na^+, Ca^{2+}, and K^+ channels. *Soc. Gen. Physiol. Ser.* 50:1–16.

Hess, P. 1987. Elementary properties of cardiac calcium channels: a brief review. *Can. J. Physiol. Pharmacol.* 66:1218–1223.

Hess, P., J. B. Lansman, and R. W. Tsien. 1986. Calcium channel selectivity for divalent and monovalent cations: voltage and concentration dependence of single channel current in ventricular heart cells. *J. Gen. Physiol.* 88:293–319.

Hess, P., and R. W. Tsien. 1984. Mechanism of ion permeation through calcium channels. *Nature.* 309:453–456.

Hoyles, M., S. Kuyucak, and S. H. Chung. 1996. Energy barrier presented to ions by the vestibule of the biological membrane channel. *Biophys. J.* 70:1628–1642.

Hoyles, M., S. Kuyucak, and S. H. Chung. 1998a. Computer simulation of ion conductance in membrane channels. *Phys. Rev. E.* 58:3654–3661.

Hoyles, M., S. Kuyucak, and S. H. Chung. 1998b. Solutions of Poisson's equation in channel-like geometries. *Computer Phys. Commun.* 115: 45–68.

Im, W., S. Seefeld, and B. Roux. 2000. A grand canonical Monte Carlo-Brownian dynamics algorithm for simulating ion channels. *Biophys. J.* 79:788–801.

Kim, M. S., T. Morii, L. X. Sun, K. Imoto, and Y. Mori. 1993. Structural determinants of ion selectivity in brain calcium channel. *FEBS Lett.* 318:145–148.

Kostyuk, P. G., S. L. Mironov, and Y. M. Shuba. 1983. Two ion-selecting filters in the calcium channel of the somatic membrane of mollusk neurons. *J. Membr. Biol.* 76:83–93.

Kuo, C. C., and P. Hess. 1992. A functional view of the entrances of L-type Ca^{2+} channels: estimates of the size and surface potential at the pore mouths. *Neuron.* 9:515–526.

Kuo, C. C., and P. Hess. 1993a. Ion permeation through the L-type Ca^{2+} channel in rat phaeochromocytoma cells: two sets of ion binding sites in the pore. *J. Physiol.* 466:629–655.

Kuo, C. C., and P. Hess. 1993b. Characterization of the high-affinity Ca^{2+} binding sites in the L-type Ca^{2+} channel pore in rat phaeochromocytoma cells. *J. Physiol.* 466:657–682.

Lansman, J. B., P. Hess, and R. W. Tsien. 1986. Blockade of current through single calcium channels by Cd^{2+}, Mg^{2+}, and Ca^{2+}: voltage and concentration dependence of calcium entry into the pore. *J. Gen. Physiol.* 88:321–347.

Levitt, D. G. 1978. Electrostatic calculations for an ion channel. I. Energy and potential profiles and interactions between ions. *Biophys. J.* 22: 209–219.

Li, S. C., M. Hoyles, S. Kuyucak, and S. H. Chung. 1998. Brownian dynamics study of ion transport in the vestibule of membrane channels. *Biophys. J.* 74:37–47.

Lux, H. D., E. Carbone, and H. Zucker. 1990. Na^+ currents through low-voltage-activated Ca^{2+} channels of chick sensory neurons: block by external Ca^{2+} and Mg^{2+}. *J. Physiol.* 430:159–188.

Lynden-Bell, R. M., and J. C. Rasaiah. 1996. Mobility and solvation of ions in channels. *J. Chem. Phys.* 105:9266–9280.

Lyubartsev, A. P., and A. Laaksonen. 1995. Calculation of the effective interaction potentials from radial distribution functions: a reverse Monte Carlo approach. *Phys. Rev. E.* 52:3730–3737.

McCleskey, E. W. 1999. Calcium channel permeation: a field in flux. *J. Gen. Physiol.* 113:765–772.

McCleskey, E. W., and W. Almers. 1985. The Ca channel in skeletal muscle is a large pore. *Proc. Natl. Acad. Sci. U.S.A.* 82:7149–7153.

Mikami, A., K. Imoto, T. Tanabe, T. Niidome, Y. Mori, H. Takeshima, S. Narumiya, and S. Numa. 1989. Primary structure and functional expression of the cardiac dihydropyridine-sensitive calcium channel. *Nature.* 340:230–233.

Miller, C. 1999. Ionic hopping defended. *J. Gen. Physiol.* 113:783–787.

Morrill, J. A., and R. MacKinnon. 1999. Isolation of a single carboxyl-carboxylate proton binding site in the pore of a cyclic nucleotide-gated channel. *J. Gen. Physiol.* 114:71–83.

Moy, G., B. Corry, S. Kuyucak, and S. H. Chung. 2000. Tests of continuum theories as models of ion channels: I. Poisson-Boltzmann theory versus Brownian dynamics. *Biophys. J.* 78:2349–2363.

Nilius, B., P. Hess, J. B. Lansman, and R. W. Tsien. 1985. A novel type of cardiac calcium channel in ventricular cells. *Nature.* 316:443–446.

Nonner, W., and B. Eisenberg. 1998. Ion permeation and glutamate residues linked by Poisson-Nernst-Planck theory in L-type calcium channels. *Biophys. J.* 75:1287–1305.

Parent, L., and M. Gopalakrishnan. 1995. Glutamate substitution in repeat IV alters divalent and monovalent cation permeation in the heart Ca^{2+} channel. *Biophys. J.* 69:1801–1813.

Polo-Parada, L., and S. J. Korn. 1997. Block of N-type calcium channels in chick sensory neurons by external sodium. *J. Gen. Physiol.* 109: 693–702.

Root, M. J., and R. MacKinnon. 1994. Two identical noninteracting sites for an ion channel revealed by proton transfer. *Science.* 265:1852–1856.

Rosenberg, R. L., and X. H. Chen. 1991. Characterization and localization of two ion-binding sites within the pore of cardiac L-type calcium channels. *J. Gen. Physiol.* 97:1207–1225.

Rosenberg, R. L., P. Hess, J. P. Reeves, H. Smilowitz, and R. W. Tsien. 1986. Calcium channels in planar lipid bilayers: insights into mechanisms of ion permeation and gating. *Science.* 231:1564–1566.

Roux, B., and M. Karplus. 1991. Ion transport in a gramicidin-like channel: dynamics and mobility. *J. Phys. Chem.* 95:4856–4868.

Roux, B., and R. MacKinnon. 1999. The cavity and pore helices in the KcsA K^+ channel: electrostatic stabilization of monovalent cations. *Science.* 285:100–102.

Sansom, M. S. P., G. R. Smith, C. Adcock, and P. C. Biggin. 1997. The dielectric properties of water within model transbilayer pores. *Biophys. J.* 73:2404–2415.

Schetz, J. A., and P. A. V. Anderson. 1993. A reevaluation of the structure of the pore region of voltage activated cation channels. *Biol. Bull.* 185:462–466.

Smith, G. R., and M. S. P. Sansom. 1997. Dynamic properties of Na^+ ions in models of ion channels: a molecular dynamics study. *Biophys. J.* 75:2767–2782.

Smith, G. R., and M. S. P. Sansom. 1999. Effective diffusion coefficients of K^+ and Cl^- ions in ion channel models. *Biophys. Chem.* 79:129–151.

Stillinger, F. H., and A. Rahman. 1974. Improved simulation of liquid water by molecular dynamics. *J. Chem. Phys.* 60:1545–1557.

Tanabe, T., H. Takeshima, A. Mikami, V. Flockerzi, K. Takahashi, K. Kangawa, M. Kojima, H. Matsuo, T. Hirose, and S. Numa. 1987. Primary structure of the receptor for calcium channel blockers from skeletal muscle. *Nature.* 328:313–318.

Tsien, R. W., P. Hess, E. W. McCleskey, and R. L. Rosenberg. 1987. Calcium channels: mechanisms of selectivity, permeation and block. *Annu. Rev. Biophys. Chem.* 16:265–290.

van Gunsteren, W. F., and H. J. C. Berendsen. 1982. Algorithms for Brownian dynamics. *Mol. Phys.* 45:637–647.

Williams, M. E., P. F. Brust, D. H. Feldman, S. Patthi, S. Simerson, A. Maroufi, A. F. McCue, G. Velicelebi, S. B. Ellis, and M. M. Harpold. 1992. Structure and functional expression of an omega-conotoxin-sensitive human N-type calcium channel. *Science.* 257:389–395.

Yang, J., P. T. Ellinor, W. A. Sather, J. F. Zhang, and R. W. Tsien. 1993. Molecular determinants of Ca^{2+} selectivity and ion permeation in L-type Ca^{2+} channels. *Nature.* 366:158–161.

Zhang, L., H. T. Davis, D. M. Kroll, and H. S. White. 1995. Molecular dynamics simulations of water in a spherical cavity. *J. Phys. Chem.* 99:2878–2884.